

We again sincerely thank both reviewers for taking the time to review and improve the paper. We hope that we satisfactorily address the various comments and questions below (responses in blue).

**Reviewer 1:**

"GENERAL COMMENTS

The authors have addressed most of my previous comments. In the discussion of the differences between model results and data-driven estimates there could be a clarification in the comparison of numbers (see below). Also I do not agree with the way the authors dismiss differences in  $k$  to explain the divergence of results. Changes in  $k$  will lead to changes in emissions if the water is substantially over-saturated in  $\text{CO}_2$  (the change of  $k$  will have a small effect of the flux, in the water is very close to saturation, which is not the case of the Congo). I suggest that the authors provide a sensitivity analysis and increase the  $k$  by 50% and see how much the flux changes in the Congo, rather than refer to a study in the Amazon.

MAJOR COMMENTS

L78 : Battin et al (2009) report on aquatic heterotrophy (respiration) not C transfer to LOAC

Ok thanks, we realised that the transfer to LOAC quoted in Battin et al. (2009) is directly taken from Tranvik et al. (2009) so we have replaced former with the latter.

L 391 : The comparison of  $\text{pCO}_2$  in the main-stem Congo at Kisangani and Kinshasa does allow to conclude that the model reproduces the "broad spatial pattern of  $\text{pCO}_2$  measured in Borges et al. (2019)" as stated. There are other important features of "spatial pattern" of  $\text{pCO}_2$  observations such as much higher  $\text{pCO}_2$  values in the small and major tributaries in some cases with  $\text{pCO}_2$  values up to 18,000 ppm. I suggest to rephrase to "broad spatial pattern of  $\text{pCO}_2$  measured in the main-stem Congo reported by Borges et al. (2019)"

This is a fair point, we have rephrased as you suggested.

L409 : Borges et al. (2019) (Figure 20) also reports a 2 yr time series (2017-2018) of  $\text{pCO}_2$  at Kisangani. Wang et al. (2013) report a 1 yr time series of  $\text{pCO}_2$  at Kinshasa. It would make a convincing case if the time-series comparison was extended to these 2 other sites were complete annual cycles are available rather than only to Bangui on the basis that is the "most complete" as stated (whatever "complete" means in this context).

Thanks for these suggestions. We have tried to access the time series from both Borges et al. (2019) and Wang et al. (2013) but have been unable to access these publicly. Borges et al. (2019) uploaded two spreadsheets publicly detailing both their continuous and discrete measurements of  $\text{pCO}_2$  (<https://zenodo.org/record/3413449#.XYm2eUYzaUk>) but neither spreadsheet contains the time series at Kisangani. Nor does the supplementary data from [Borges et al. \(2015\)](#) contain a full time series.

If necessary, we would be happy to contact the authors of these studies directly but would require a longer extension and even then, we cannot be sure whether we would get access to these datasets.

We have at least been able to compare values for December and June at Kisangani (see Table 3).

L 584 : The value of  $k$  of 3.5 m/d is ok for high order streams (for instance minstem) and  $k$  used by Borges et al (2019) strongly increases in low order streams up to 39 m/d in order 1 streams. The largest fraction of CO<sub>2</sub> emission reported by Borges et al. (2019) from the river network is related to low order streams.

L 587 : The statement that CO<sub>2</sub> flux in orchileak is not sensitive to the  $k$  value is really strange and might require a few words of explanation. For a water pCO<sub>2</sub> of 2800 ppm (seems to be sort of simulated pCO<sub>2</sub> by the model in the Congo river) and a  $k$  of 3.5 m/d, the emission is more or less 287 mmol/m<sup>2</sup>/d. If the  $k$  is increased by 50% (=5.3 m/d) the resulting flux is more or less 430 mmol/m<sup>2</sup>/d, so also 50% higher.

So whether the fluxes are derived from ORCHILEAK or “data-driven models”, a substantial increase of  $k$  leads to a substantial increase of  $k$ . I suggest that the authors provide a sensitivity analysis and increase the  $k$  by 50% in Orchileak and see how much the flux changes in the Congo, rather than refer to a study in the Amazon.

Based on the reported values of flux,  $k$  and surface area, I compute that the spatially integrated average of river pCO<sub>2</sub> from ORCHILEAK is approximately 2800 ppm. The spatially integrated average of river pCO<sub>2</sub> from Borges et al (2019) is approximately 5560 ppm based on numbers in Table 1. The average  $k$  Borges et al (2019) is 8 m/d, also based on data from Table 1, which is higher than the  $k$  value in ORCHILEAK of 3.5 m/d. So the difference between both estimates is related to both lower pCO<sub>2</sub> and lower  $k$  in Orchileak. The authors should clarify how  $K$  is computed in Orchileak and discuss in light of the  $k$  computation scheme of Borges et al. (2019) that is transparently explained in the methods and supplements. This might shed some light on why the  $k$  values are so different in both studies. The higher pCO<sub>2</sub> values in Borges et al. (2019) might result from not representing macrophytes and/or because the model under-estimates pCO<sub>2</sub> in low order streams. This is not possible to check since the model results are presented as overall means and not information is given as function of stream size. I suggest that the authors present in more detail the pCO<sub>2</sub> values simulated to tributaries and in particular low or der streams.

While possible, we would maintain that a bespoke sensitivity analysis of  $k$  for the Congo is unnecessary. As shown in the sensitivity analysis of Lauerwald et al. (2017),  $FCO_2$  in ORCHILEAK (as a process based/ physical approach) is not sensitive to  $k$  due to the following:

-  $FCO_2$  at a particular 6-min timestep is indeed calculated based on the water-atmosphere pCO<sub>2</sub> gradient, the water surface area and  $k$  (see equations 76 and 77 of Lauerwald et al., 2017). As outlined in the methods section, in ORCHILEAK fixed  $k$  values of 3.5 m d<sup>-1</sup> and 0.65 m d<sup>-1</sup> respectively are used for rivers (including open floodplains) and forested floodplains, the former similar to the 2.9 m d<sup>-1</sup> for rivers used by Borges et al. (2015<sup>a</sup>).

-In turn, at each time-step  $p\text{CO}_2$  in the water column is calculated from the concentration of dissolved  $\text{CO}_2$  and the temperature-dependent solubility of carbon (see equation 70). The concentration of dissolved  $\text{CO}_2$  in turn depends on the input and decomposition of DOC (in situ production of  $\text{CO}_2$ ) and the input of dissolved  $\text{CO}_2$  from soils, litter and root respiration (see various equations from 58-69) on the input side, and the velocity  $k$  that controls how quickly these  $\text{CO}_2$  inputs can diffuse to the atmosphere.

-In ORCHILEAK,  $k$  does have an important impact on  $p\text{CO}_2$ ; i.e. a lower  $k$  value will increase  $p\text{CO}_2$ , but this will also lead to a steeper water-air  $\text{CO}_2$  gradient and so ultimately to approximately the same  $F\text{CO}_2$  over time. In other words, over the scales covered in this research (the large catchment area and water residence times of the Congo),  $F\text{CO}_2$  is ultimately mainly controlled by the allochthonous inputs of carbon to the river network, because by far the largest fraction of these C inputs is leaving the system via  $\text{CO}_2$  emission to the atmosphere (as opposed to being laterally transferred downstream). The Cuvette Centrale is a hotspot region for  $F\text{CO}_2$  (see Figure 8) due to the high allochthonous inputs of C to the river network, not due to particularly high or low  $k$  values.

As a process-based model, ORCHILEAK represents directly the sources of C to the river network, and these are the main drivers of  $\text{CO}_2$  emissions. In empirical studies, on the contrary, you don't know the C sources to the river with which to constrain  $\text{CO}_2$  emissions; what is measured is the  $p\text{CO}_2$ , and you have to estimate the  $k$  that has led to this  $p\text{CO}_2$  under an unknown  $\text{CO}_2$  input/production.

We absolutely take your point that further explanation is required and in line with the above, have changed the text in the manuscript as follows (Lines 590-610):

“One potential cause for the differences could be the river gas exchange velocity  $k$ . We applied a mean riverine gas exchange velocity  $k_{600}$  of  $3.5 \text{ m d}^{-1}$  which is similar to the  $2.9 \text{ m d}^{-1}$  used by Borges et al. (2015<sup>a</sup>) but substantially smaller than the mean of approximately  $8 \text{ m d}^{-1}$  estimated across Strahler orders 1-10 in Borges et al. (2019) (taking the contributing water surface area of each Strahler order into account). A sensitivity analysis was performed in Lauerwald et al. (2017) which showed that in the physical approach of ORCHILEAK,  $\text{CO}_2$  evasion is not very sensitive to the  $k$  value, unlike data-driven models. Namely, Lauerwald et al (2017) showed that an increase or decrease of  $k_{600}$  for rivers and swamps (flooded forests) of 50% only led to 1% and -4% change in total  $\text{CO}_2$  evasion, respectively. In ORCHILEAK,  $k$  does have an important impact on  $p\text{CO}_2$ ; i.e. a lower  $k$  value will increase  $p\text{CO}_2$ , but this will also lead to a steeper water-air  $\text{CO}_2$  gradient and so ultimately to approximately the same  $F\text{CO}_2$  over time. In other words, over the scales covered in this research (the large catchment area and water residence times of the Congo),  $F\text{CO}_2$  is mainly controlled by the allochthonous inputs of carbon to the river network, because by far the largest fraction of these C inputs is leaving the system via  $\text{CO}_2$  emission to the atmosphere (as opposed to being laterally transferred downstream). Therefore, we do not consider  $k$  to be a major source of the discrepancy. Additionally, our  $k_{600}$  value of  $0.65 \text{ m d}^{-1}$  for forested floodplains (based on Richey et al., 2002) compares well to recent a study which directly measured  $k_{600}$  on two different flooded forest sites in the Amazon basin, observing a range of  $0.24$  to  $1.2 \text{ m d}^{-1}$  (MacIntyre et al., 2019).”

L 578 comparison with Lauerwald et al. (2015) also suggests that you « substantially underestimate total riverine CO<sub>2</sub> evasion”.

This is true, though I think this is already acknowledged in the preceding sentence “but smaller than the 59.7 Tg C yr<sup>-1</sup> calculated by Lauerwald et al. (2015) and far smaller than that of Borges et al. (2015<sup>a</sup>), 133-177 Tg C yr<sup>-1</sup> or Borges et al. (2019), 251±46 Tg C yr<sup>-1</sup>.”

Regarding historical changes in LOAC fluxes, the authors might consider including in the discussion the recent paper of Moukandi N’kaya et al. (2020) that attribute decadal changes in DOC export from the Congo to changes in hydrology and inundation patterns.

Thank you for pointing out this paper. We have added a new paragraph to the discussion as follows (721-736):

“With these limitations in our understanding of tropical forest ecosystems in mind, over the entire simulation period (1861-2099) we estimate that aquatic CO<sub>2</sub> evasion will increase by 79% and the export of C to the coast by 67%. While, there are no long-term observations of aquatic CO<sub>2</sub> evasion in the Congo, a recent paper examined trends in observed DOC fluxes in the Congo at Brazzaville/Kinshasa over the last 30 years (Moukandi N’kaya et al. 2020). They found a 45% increase in the annual flux of DOC from 11.1 Tg C yr<sup>-1</sup> (mean from 1987-1993) to 16.1 Tg C yr<sup>-1</sup> (mean from 2006-2017). Comparing the same two periods, we find a smaller increase of 15% from 12.3 Tg C yr<sup>-1</sup> to 14.2 Tg C yr<sup>-1</sup>. While our increase is substantially smaller, these observations are still over relatively short time scales and thus interannual variations could have considerable influence over the means of the two periods. Irrespectively it is encouraging that observations concur with the overall simulated increasing trend. Perhaps most interesting is that Moukandi N’kaya et al. (2020) attribute this increase to hydrological changes and specifically an increase in flood events in the central basin (including the Cuvette Centrale). Over this period, we too attribute the increase in carbon fluxes to the coast in part to climate change (Fig. 11 d) and over the full simulation period, the largest increase in DOC and CO<sub>2</sub> leaching into the aquatic system occurs within the Cuvette Centrale (Fig. A1).”

## REFS

Moukandi N’kaya et al. (2020) Temporal Variability of Sediments, Dissolved Solids and Dissolved Organic Matter Fluxes in the Congo River at Brazzaville/Kinshasa, *Geosciences* 2020, 10, 341; doi:10.3390/geosciences10090341

Wang, Z. A., D. J. Bienvenu, P. J. Mann, K. A. Hoering, J. R. Poulsen, R. G. M. Spencer, and R. M. Holmes (2013), Inorganic carbon speciation and fluxes in the Congo River, *Geophys. Res. Lett.*, 40, doi:10.1002/grl.50160"

## Reviewer 2:

"Hastie and co-authors have responded well to comments on their initial submission. Though their projections of changes through this century are more uncertain and speculative than as suggested in the abstract, the main text does acknowledge the considerable problems with the projections. The following specific comments are minor or can be readily clarified.

Introduction

L49: Change 'sparsity' to 'paucity'.

Thanks, changed as suggested.

Methods

L140-142: 'Fixed gas exchange velocities of 3.5 m d<sup>-1</sup> and 0.65 m d<sup>-1</sup> respectively. are used for rivers (including open floodplains) and forested floodplains.'

A couple of references for these gas exchange velocities could be added. In particular, MacIntyre et al (2019) provides results for forested floodplains.

MacIntyre et al. 2019. Turbulence and gas transfer velocities in sheltered flooded forests of the Amazon basin. *Geophysical Research Letters*. doi.org/10.1029/2019GL083948

Thanks for pointing out this additional reference. MacIntyre et al. (2019) measured gas transfer velocities on two flooded forest sites in the Amazon ranging from 0.24 to 1.2 m d<sup>-1</sup> so our value of 0.65 m d<sup>-1</sup> lies in the middle of this range.

We have modified the text (lines 590-610) as follows (also to address the comments of Reviewer 1):

"One potential cause for the differences could be the river gas exchange velocity  $k$ . We applied a mean riverine gas exchange velocity  $k_{600}$  of 3.5 m d<sup>-1</sup> which is similar to the 2.9 m d<sup>-1</sup> used by Borges et al. (2015<sup>a</sup>) but substantially smaller than the mean of approximately 8 m d<sup>-1</sup> estimated across Strahler orders 1-10 in Borges et al. (2019) (taking the contributing water surface area of each Strahler order into account). A sensitivity analysis was performed in Lauerwald et al. (2017) which showed that in the physical approach of ORCHILEAK, CO<sub>2</sub> evasion is not very sensitive to the  $k$  value, unlike data-driven models. Namely, Lauerwald et al (2017) showed that an increase or decrease of  $k_{600}$  for rivers and swamps (flooded forests) of 50% only led to 1% and -4% change in total CO<sub>2</sub> evasion, respectively. In ORCHILEAK,  $k$  does have an important impact on  $p\text{CO}_2$ ; i.e. a lower  $k$  value will increase  $p\text{CO}_2$ , but this will also lead to a steeper water-air CO<sub>2</sub> gradient and so ultimately to approximately the same  $F\text{CO}_2$  over time. In other words, over the scales covered in this research (the large catchment area and water residence times of the Congo),  $F\text{CO}_2$  is mainly controlled by the allochthonous inputs of carbon to the river network, because by far the largest fraction of these C inputs is leaving the system via CO<sub>2</sub> emission to the atmosphere (as opposed to being laterally transferred downstream). Therefore, we do not consider  $k$  to be a major source of the discrepancy. Additionally, our  $k_{600}$  value of 0.65 m d<sup>-1</sup> for forested floodplains (based on Richey et al., 2002) compares well to recent a study which directly measured  $k_{600}$  on two different flooded forest sites in the Amazon basin, observing a range of 0.24 to 1.2 m d<sup>-1</sup> (MacIntyre et al., 2019)."

Figure 3a: Are fluxes from L. Tanganyika and other lakes included? If so, what is the source of the gas concentrations and fluxes.

No, as lakes are not directly represented in ORCHILEAK.

L241-242: 'The best performing climate forcing dataset was ISIMIP2b followed by Princeton GPCP with root mean square errors (RMSE) of 29% and 40% and Nash Sutcliffe efficiencies (NSE) of 0.20 and -0.25, respectively.'

Are RMSE and NSE values considered fair or good?

As the other reviewer previously pointed out, I suppose this is for the reader to decide. Also, these values are before calibration (the metrics for ISIMIP improve after calibration).

248-250: 'water residence times - 0.5 (days) for floodplain reservoirs'

What is the basis for residence times of 0.5 days on the floodplains, as it seems too fast?

The 0.5 days actually refers to  $\tau_{\text{flood}}$  ( $\tau_{\text{flood}}$ ), a parameter which helps to control the residence time. However, this parameter is multiplied by a topographical index and the flooded fraction of the grid cell to calculate residence time, and residence time is thus changing at each time step but is not explicitly calculated as diagnostic output variable. The  $\tau_{\text{flood}}$  value of 0.5 was arrived at by calibrating against two very different rivers (the Congo and the Oubangui) and flooded seasonality (GIEMS), as well as trying to represent a large and diverse basin.

We apologise for the mistake in the manuscript and the confusion caused. We have changed the text as follows (247-256):

"For ISIMIP2b we further calibrated key hydrological model parameters, namely the constants ( $\tau$ ,  $\tau$ ) which help to control the water residence time of the groundwater (=slow reservoir), headwaters (= fast reservoir) and floodplain reservoirs in order to improve the simulation of observed discharge at Brazzaville and Oubangui (Table 2). To do so, we tested different combinations of  $\tau$  values for the three reservoirs, eventually settling on 1, 0.5 and 0.5 (days) for the slow, fast and floodplain reservoirs respectively, all three being reduced compared to those values used in the original ORCHILEAK calibration for the Amazon (Lauerwald et al., 2017). The actual residence time of each reservoir is calculated at each time step. The residence time of the flooded reservoir for example, is a product of  $\tau_{\text{flood}}$ , a topographical index and the flooded fraction of the grid cell."

L255-257: 'As in previous studies on the Amazon basin (Lauerwald et al. 2017, Hastie et al., 2019) we defined bank-full discharge, i.e. the threshold discharge at which floodplain inundation starts (i.e. overtopping of banks), as the median discharge (50th percentile) of the present-day climate forcing period (1990 to 2005).'

The response to the comment on the initial submission ('The concept of bank-full discharge as a threshold for initiation of inundation of floodplains is questionable as applied to tropical



floodplain such as those in the Amazon or Congo. Studies inundation dynamics in the Amazon with detailed measurements or modeling indicate that inundation occurs more or less continuously as the rivers rise and that the water comes from both the rivers and uplands.’) was mis-interpreted. The issue being raised was with regard to the proportion of water from different sources. The issue concerns the observation that natural floodplains, such as those in the Amazon and Congo, have channels that connect the rivers to the floodplains such that waters rise on the floodplains in concert with the river rise, not just after bank-full discharge is reached.

Ok, we understand now. In regards to this, ORCHILEAK simulates both precipitation onto the floodplain and evaporation from the floodplain. This precipitation in turn feeds directly into the floodplain reservoir and thus in ORCHILEAK inundation on the floodplain is not only a result of overtopping but also local precipitation directly onto the floodplain.

Table 1: Is there snowfall in basin?

No, I don't think there is, good point. We have deleted reference to this in the Table

How does the river area used compare to the recent estimate by Allen and Pavelsky (2018. Global extend of rivers and streams. Science 361: 585–588) ?

According to their summary shapefile per basin (downloaded here- <https://drive.google.com/file/d/11hzVVg6OEs1c7zIKjuy0u4WeE0UG6BsH/view>) Allen and Pavelsky estimate a total river and stream surface area of 17,903 km<sup>2</sup> for the Congo basin, which falls at the lower end when compared to existing estimates such as 23,670 km<sup>2</sup> from Borges et al. (2019) and 26,517 km<sup>2</sup> from Borges et al. (2015, based on Raymond et al., 2013). While this may indicate that both our estimate and that of Borges et al. (2019) are too high, that is not the reason for the discrepancy between our FCO<sub>2</sub> and Borges' given that our estimates are relatively similar.

We have added a sentence on this (611-616):

“Another potential reason for our smaller riverine CO<sub>2</sub> evasion could be river surface area. We simulate a mean present day (1980-2010) total river surface area of 25,900 km<sup>2</sup>, compared to the value of 23,670 km<sup>2</sup> used in Borges et al (2019, supplementary information) and so similarly we think that this can be discounted as a major source of discrepancy. However, it should be noted that both estimates are high compared to the recent estimate of 17,903 km<sup>2</sup> based on analysis of Landsat images (Allen & Pavelsky, 2018).”

Results

Table 2: State 'observed flooded area' is from GIEMS. As noted correctly in the text (L364-379), the GIEMS data under-estimate the flooded area.

Changed as suggested: “Observed flooded area is from GIEMS (Papa et al., 2010, Becker et al., 2018).”

L448-449: 'We simulate a mean annual flux of DOC throughfall from the canopy of  $27 \pm 1$  Tg C yr<sup>-1</sup>. How does this compare to measured fluxes (e.g. Filoso et al. 1999. Composition and deposition of throughfall in a flooded forest archipelago (Anavilhanas, Negro River, Brazil). Biogeochemistry 45:169-195)."

This paper (Filoso et al., 1999) was indeed used in the ORCHILEAK model development paper (Lauerwald et al., 2017) for validation of throughfall and it compared well. Please see Figure 11 and Table 2 of Lauerwald et al., 2017.



# 1 **Historical and future contributions of inland waters to the Congo basin**

## 2 **carbon balance**

3 Adam Hastie<sup>1,2</sup>, Ronny Lauerwald<sup>2,3,4</sup>, Philippe Ciais<sup>3</sup>, Fabrice Papa<sup>5,6</sup>, Pierre Regnier<sup>2</sup>

4

5 <sup>1</sup>School of GeoSciences, University of Edinburgh, EH9 3FF, Edinburgh, Scotland, UK

6 <sup>2</sup>Biogeochemistry and Earth System Modelling, Department of Geoscience, Environment and  
7 Society, Université Libre de Bruxelles, Bruxelles, 1050, Belgium

8 <sup>3</sup>Laboratoire des Sciences du Climat et de l'Environnement (LSCE), CEA CNRS UVSQ, Gif-  
9 sur-Yvette 91191, France

10 <sup>4</sup>Université Paris-Saclay, INRAE, AgroParisTech, UMR ECOSYS, 78850, Thiverval-Grignon,  
11 France

12 <sup>5</sup>Laboratoire d'Etudes en Géophysique et Océanographie Spatiales, Centre National de la  
13 Recherche Scientifique–Institut de recherche pour le développement–Université Toulouse Paul  
14 Sabatier–Centre national d'études spatiales, 31400 Toulouse, France

15 <sup>6</sup>~~UnB, Universidade de Brasília, Institute of Geosciences, Campus Universitario Darcy Ribeiro,~~  
16 ~~70910-900 Brasilia (DF), Brazil~~~~Indo-French Cell for Water Sciences, International Joint~~  
17 ~~Laboratory Institut de Recherche pour le Développement and Indian Institute of~~  
18 ~~Science, Indian Institute of Science, 560012 Bangalore, India~~

19

20 *Correspondence to:* Adam Hastie (adam.hastie@ed.ac.uk)

21

## 22 **Abstract**

23 As the second largest area of contiguous tropical rainforest and second largest river basin in  
24 the world, the Congo basin has a significant role to play in the global carbon (C) cycle. For the  
25 present day, it has been shown that a significant proportion of global terrestrial net primary  
26 productivity (NPP) is transferred laterally to the land-ocean aquatic continuum (LOAC) as  
27 dissolved CO<sub>2</sub>, dissolved organic carbon (DOC) and particulate organic carbon (POC). Whilst  
28 the importance of LOAC fluxes in the Congo basin has been demonstrated for the present day,  
29 it is not known to what extent these fluxes have been perturbed historically, how they are likely  
30 to change under future climate change and land use scenarios, and in turn what impact these  
31 changes might have on the overall C cycle of the basin. Here we apply the ORCHILEAK model  
32 to the Congo basin and estimate that 4% of terrestrial NPP (NPP = 5,800 ±166 Tg C yr<sup>-1</sup>) is

33 currently exported from soils and vegetation to inland waters. Further, our results suggest that  
34 aquatic C fluxes may have undergone considerable perturbation since 1861 to the present day,  
35 with aquatic CO<sub>2</sub> evasion and C export to the coast increasing by 26% (186 ±41 Tg C yr<sup>-1</sup> to  
36 235 ±54 Tg C yr<sup>-1</sup>) and 25% (12 ±3 Tg C yr<sup>-1</sup> to 15 ±4 Tg C yr<sup>-1</sup>) respectively, largely because  
37 of rising atmospheric CO<sub>2</sub> concentrations. Moreover, under climate scenario RCP 6.0 we  
38 predict that this perturbation could continue; over the full simulation period (1861-2099), we  
39 estimate that aquatic CO<sub>2</sub> evasion and C export to the coast could increase by 79% and 67%  
40 respectively. Finally, we show that the proportion of terrestrial NPP lost to the LOAC could  
41 increase from approximately 3% to 5% from 1861-2099 as a result of increasing atmospheric  
42 CO<sub>2</sub> concentrations and climate change. However, our future projections of the Congo basin C  
43 fluxes in particular need to be interpreted with some caution due to model limitations. We  
44 discuss these limitations, including the wider challenges associated with applying the current  
45 generation of land surface models which ignore nutrient dynamics to make future projections  
46 of the tropical C cycle, along with potential next steps.

## 47 **1. Introduction**

48 As the world's second largest area of contiguous tropical rainforest and second largest river,  
49 the Congo basin has a significant role to play in the global carbon (C) cycle. Current estimates  
50 of its C stocks and fluxes are limited by a sparsity-paucity of field data and therefore have  
51 substantial uncertainties, both quantified and unquantified (Williams et al., 2007; Lewis et al.,  
52 2009; Dargie et al., 2017). Nevertheless, it has been estimated that there is approximately 50  
53 Pg C stored in its above ground biomass (Verhegghen et al., 2012), and up to 100 Pg C  
54 contained within its soils (Williams et al., 2007). Moreover, a recent study estimated that  
55 around 30 (6.3–46.8) Pg C is stored in the peats of the Congo alone (Dargie et al., 2017). Field  
56 data suggest that storage in tree biomass increased by 0.34 (0.15- 0.43) Pg C yr<sup>-1</sup> in intact  
57 African tropical forests between 1968-2007 (Lewis et al., 2009) due in large part to a

58 combination of increasing atmospheric CO<sub>2</sub> concentrations and climate change (Ciais et al.,  
59 2009; Pan et al., 2015), while satellite data indicates that terrestrial net primary productivity  
60 (NPP) has increased by an average of 10 g C m<sup>-2</sup> yr<sup>-1</sup> per year between 2001 and 2013 in tropical  
61 Africa (Yin et al., 2017).

62 At the same time, forest degradation, clearing for rotational agriculture and logging are causing  
63 C losses to the atmosphere (Zhuravleva et al., 2013; Tyukavina et al., 2018) while droughts  
64 have reduced vegetation greenness and water storage over the last decade (Zhou et al., 2014).  
65 A recent estimate of above ground C stocks of tropical African forests, mainly in the Congo,  
66 indicates a minor net C loss from 2010 to 2017 (Fan et al., 2019). Moreover, recent field data  
67 suggests that the above ground C sink in tropical Africa was relatively stable from 1985 to  
68 2015 (Hubau et al., 2020).

69 There are large uncertainties associated with projecting future trends in the Congo basin  
70 terrestrial C cycle, firstly related to predicting which trajectories of future CO<sub>2</sub> levels and land  
71 use changes will occur, and secondly to our ability to fully understand and simulate these  
72 changes and in turn their impacts. Future model projections for the 21<sup>st</sup> century agree that  
73 temperature will significantly increase under both low and high emission scenarios (Haensler  
74 et al., 2013), while precipitation is only projected to substantially increase under high emission  
75 scenarios, the basin mean remaining more or less unchanged under low emission scenarios  
76 (Haensler et al., 2013). Uncertainties in future land-use change projections for Africa are  
77 among the highest for any continent (Hurt et al., 2011).

78 For the present day at the global scale, it has been estimated that between 1 and 5 Pg C yr<sup>-1</sup> is  
79 transferred laterally to the land-ocean aquatic continuum (LOAC) as dissolved CO<sub>2</sub>, dissolved  
80 organic carbon (DOC) and particulate organic carbon (POC) (Cole et al., 2007; [Tranvik](#)~~Battin~~  
81 et al., 2009; Regnier et al., 2013; Drake et al., 2018; Ciais et al. 2020). This C can subsequently

82 be evaded back to the atmosphere as CO<sub>2</sub>, undergo sedimentation in wetlands and inland  
83 waters, or be transported to estuaries or the coast. The tropical region is a hotspot area for  
84 inland water C cycling (Richey et al., 2002; Melack et al., 2004; Abril et al., 2014; Borges et  
85 al., 2015<sup>a</sup>; Lauerwald et al., 2015) due to high terrestrial NPP and precipitation, and a recent  
86 study used an upscaling approach based on observations to estimate present day CO<sub>2</sub> evasion  
87 from the rivers of the Congo basin at 251±46 Tg C yr<sup>-1</sup> and the lateral C (TOC +DIC) export  
88 to the coast at 15.5 (13-18) Tg C yr<sup>-1</sup> (Borges et al., 2015<sup>a</sup>; Borges et al., 2019). To put this into  
89 context, their estimate of aquatic CO<sub>2</sub> evasion represents 39% of the global value estimated by  
90 Lauerwald et al. (2015, 650 Tg C yr<sup>-1</sup>) or 14% of the global estimate of Raymond et al. (2013,  
91 1,800 Tg C yr<sup>-1</sup>). Note that while Lauerwald et al. (2015) and Raymond et al. (2013) relied  
92 largely on the same database of partial pressure of CO<sub>2</sub> (*p*CO<sub>2</sub>) measurements (GloRiCh,  
93 Hartmann et al., 2014) as the basis for their estimates, they took different, albeit both  
94 empirically led approaches. Moreover, both approaches were limited by a relative paucity of  
95 data from the tropics, which also explains the high degree of uncertainty associated with our  
96 understanding of global riverine CO<sub>2</sub> evasion.

97 Whilst the importance of LOAC fluxes in the Congo basin has been demonstrated for the  
98 present day, it is not known to what extent these fluxes have been perturbed historically, how  
99 they are likely to change under future climate change and land use scenarios, and in turn what  
100 impact these changes might have on the overall C balance of the Congo. In light of these  
101 knowledge gaps, we address the following research questions:

- 102 • What is the relative contribution of LOAC fluxes (CO<sub>2</sub> evasion and C export to the  
103 coast) to the present-day C balance of the basin?
- 104 • To what extent have LOAC fluxes changed from 1860 to the present day and what are  
105 the primary drivers of this change?

- 106 • How will these fluxes change under future climate and land use change scenarios (RCP  
107 6.0 which represents the “no mitigation scenario”) and what are the limitations  
108 associated with these future projections~~implications of this change?~~  
109

110 Understanding and quantifying these long-term changes requires a complex and integrated  
111 mass-conservation modelling approach. The ORCHILEAK model (Lauerwald et al., 2017), a  
112 new version of the land surface model ORCHIDEE (Krinner et al., 2005), is capable of  
113 simulating observed terrestrial and aquatic C fluxes in a consistent manner for the present day  
114 in the Amazon (Lauerwald et al., 2017) and Lena (Bowring et al., 2019<sup>a</sup>; Bowring et al., 2019<sup>b</sup>)  
115 basins, albeit with limitations including a lack of explicit representation of POC fluxes and in-  
116 stream autotrophic production (see Lauerwald et al., 2017; Bowring et al., 2019<sup>a</sup>; Bowring et  
117 al., 2019<sup>b</sup> and Hastie et al., 2019 for further discussion). Moreover, it was recently demonstrated  
118 that this model could recreate observed seasonal and interannual variation in Amazon aquatic  
119 and terrestrial C fluxes (Hastie et al., 2019).

120 In order to accurately simulate aquatic C fluxes, it is crucial to provide a realistic representation  
121 of the hydrological dynamics of the Congo River, including its wetlands. Here, we develop  
122 new wetland forcing files for the ORCHILEAK model from the high-resolution dataset of  
123 Gumbrecht et al. (2017) and apply the model to the Congo basin. After validating the model  
124 against observations of discharge, flooded area, DOC concentrations and  $p\text{CO}_2$  for the present  
125 day, we then use the model to understand and quantify the long- term (1861-2099) temporal  
126 trends in both the terrestrial and aquatic C fluxes of the Congo Basin.

## 127 **2. Methods**

128 ORCHILEAK (Lauerwald et al., 2017) is a branch of the ORCHIDEE land surface model  
129 (LSM), building on past model developments such as ORCHIDEE-SOM (Camino Serrano,  
130 2018), and represents one of the first LSM-based approaches which fully integrates the aquatic

131 C cycle within the terrestrial domain. ORCHILEAK simulates DOC production in the canopy  
132 and soils, the leaching of dissolved CO<sub>2</sub> and DOC to the river from the soil, the mineralization  
133 of DOC, and in turn the evasion of CO<sub>2</sub> to the atmosphere from the water surface. Moreover,  
134 it represents the transfer of C between litter, soils and water within floodplains and swamps  
135 (see section 2.2). Once within the river routing scheme, ORCHILEAK assumes that the lateral  
136 transfer of CO<sub>2</sub> and DOC are proportional to the volume of water. DOC is divided into a  
137 refractory and labile pool within the river, with half-lives of 80 and 2 days respectively. The  
138 refractory pool corresponds to the combined slow and passive DOC pools of the soil C scheme,  
139 and the labile pool corresponds to the active soil pool (see section 2.4.1). The concentration of  
140 dissolved CO<sub>2</sub> and the temperature-dependent solubility of CO<sub>2</sub> are used to calculate  $p\text{CO}_2$  in  
141 the water column. In turn, CO<sub>2</sub> evasion is calculated based on  $p\text{CO}_2$ , along with a diurnally  
142 variable water surface area and a gas exchange velocity. Fixed gas exchange velocities of 3.5  
143 m d<sup>-1</sup> and 0.65 m d<sup>-1</sup> respectively are used for rivers (including open floodplains) and forested  
144 floodplains.

145 In this study, as in previous studies (Lauerwald et al., 2017, Hastie et al. 2019, Bowring et al.,  
146 2019<sup>a,b</sup>), we run the model at a spatial resolution of 1° and use the default time step of 30 min  
147 for all vertical transfers of water, energy and C between vegetation, soil and the atmosphere,  
148 and the daily time-step for the lateral routing of water. Until now, in the Tropics, ORCHILEAK  
149 has been parameterized and calibrated only for the Amazon River basin (Lauerwald et al., 2017,  
150 Hastie et al. 2019). To adapt and apply ORCHILEAK to the specific characteristics of the  
151 Congo River basin (2.1), we had to establish new forcing files representing the maximal  
152 fraction of floodplains (MFF) and the maximal fraction of swamps (MFS) (2.2) and to  
153 recalibrate the river routing module of ORCHILEAK (2.3). All of the processes represented in  
154 ORCHILEAK remain identical to those previously represented for the Amazon ORCHILEAK  
155 (Lauerwald et al., 2017; Hastie et al., 2019). In the following methodology sections, we

156 describe; 2.1- Congo basin description, 2.2- Development of floodplains and swamps forcing  
157 files, 2.3- Calibration of hydrology, 2.4- Simulation set-up, 2.5- Evaluation and analysis of  
158 simulated fluvial C fluxes, and 2.6- Calculating the net carbon balance of the Congo Basin. For  
159 a full description of the ORCHILEAK model please see Lauerwald et al. (2017).

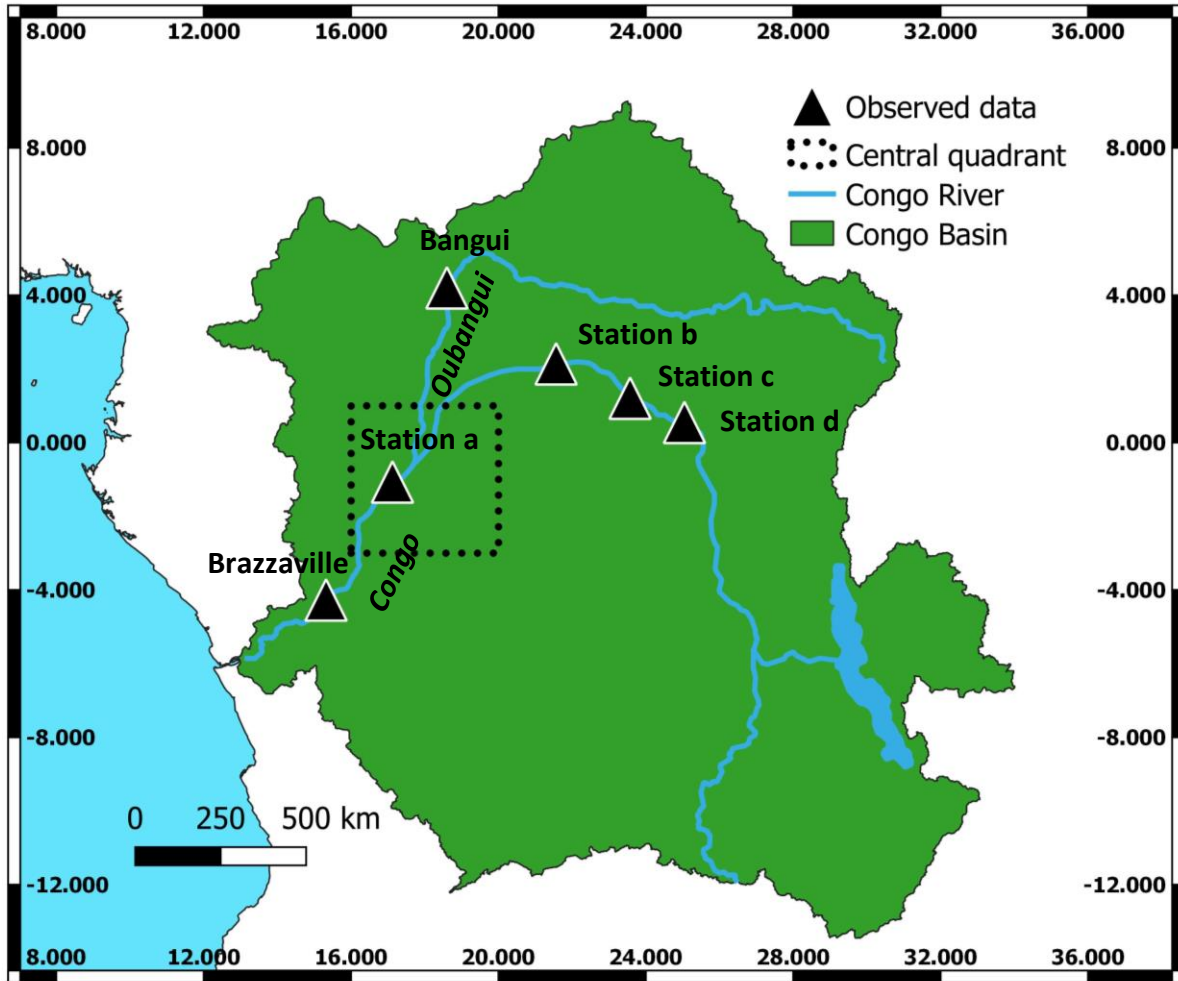
## 160 **2.1 Congo basin description**

161 The Congo Basin is the world's second largest area of contiguous tropical rainforest and second  
162 largest river basin in the world (Fig. 1), covering an area of  $3.7 \times 10^6 \text{ km}^2$ , with a mean discharge  
163 of around  $42,000 \text{ m}^3 \text{ s}^{-1}$  (O'Loughlin et al., 2013) and a variation between  $24,700\text{--}75,500 \text{ m}^3$   
164  $\text{s}^{-1}$  across months (Coynel et al., 2005).

165

166

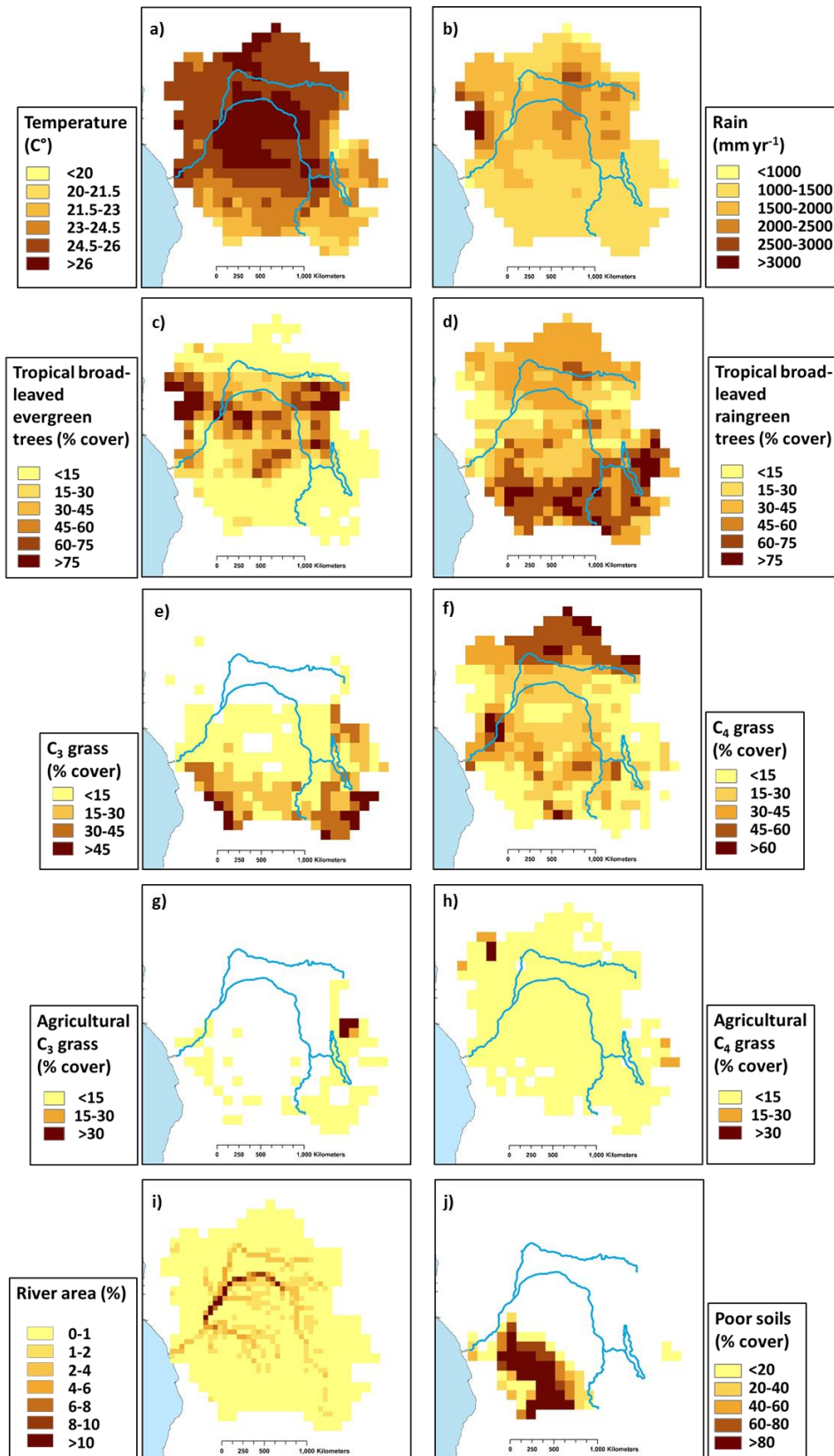




167  
 168 **Figure 1:**Extent of the Congo Basin, central quadrant of the “Cuvette Centrale” and sampling  
 169 stations (for DOC and discharge) along the Congo and Oubangui Rivers (in italic).

170  
 171 The major climate (ISMSIP2b, Frieler et al., 2017; Lang et al., 2017) and land-cover (LUH-  
 172 CMIP5) characteristics of the Congo Basin for the present day (1981-2010) are shown in Figure  
 173 2. The mean annual temperature is 25.2 °C but with considerable spatial variation from a low  
 174 of 18.4°C to a high of 27.2°C (Fig. 2 a), while mean annual rainfall is 1520mm, varying from  
 175 733 mm to 4087 mm (Fig. 2 b). ORCHILEAK prescribes 13 different plant functional types  
 176 (PFTs). Land-use is mixed with tropical broad-leaved evergreen (PFT2, Fig. 1 c), tropical  
 177 broad-leaved rain green (PFT3, Fig. 1 d), C<sub>3</sub> grass (PFT10, Fig. 2 e) and C<sub>4</sub> grass (PFT11, Fig.  
 178 2 f) covering a maximum of 26%, 35%, 8% and 25% of the basin area respectively (Table A3).  
 179 Most published estimates for land-cover follow national boundaries and so we can make broad

180 comparisons with published estimates for the Democratic Republic of Congo (DRC). For  
181 example, our value for total forest cover for the DRC (65%), is close to the 67% and 68%  
182 values estimated by the Congo Basin Forest Partnership (CBFP, 2009), and Potapov et al.  
183 (2012), respectively. Agriculture covers only a small proportion of the basin according to the  
184 LUH dataset that is based on FAO cropland area statistics, with C3 (PFT12, Fig. 2 g) and C<sub>4</sub>  
185 (PFT13, Fig. 2 h) agriculture making up a maximum basin area of 0.5 and 2% respectively. In  
186 reality, a larger fraction of the basin is composed of small scale and rotational agriculture  
187 (Tyukavina et al., 2018). The ORCHILEAK model also has a “poor soils” forcing file (Fig. 2  
188 j) which prescribes reduced decomposition rates in soils with low nutrient and pH soils such as  
189 Podzols and Arenosols (Lauerwald et al., 2017). This file is developed from the Harmonized  
190 World Soil Database (FAO/IIASA/ISRIC/ISS-CAS/JRC, 2009).



191

192 **Figure 2: Present day (1981-2010) spatial distribution of the principal climate and land-use**  
 193 **drivers used in ORCHILEAK, across the Congo Basin; a) mean annual temperature in °C, b)**  
 194 **mean annual rainfall in mm yr<sup>-1</sup>, c)-h) mean annual maximum vegetated fraction for PFTs 2,3,**

195 **10,11,12 and 13, i) river area, and j) Poor soils. All at a resolution of 1° except for river area**  
196 **(0.5°).**

## 197 **2.2 Development of floodplains and swamps forcing files**

198 In ORCHILEAK, water in the river network can be diverted to two types of wetlands,  
199 floodplains and swamps. In each grid where a floodplain exists, a temporary waterbody can be  
200 formed adjacent to the river and is fed by the river once bank-full discharge (see section 2.3)  
201 is exceeded. In grids where swamps exist, a constant proportion of river discharge is fed into  
202 the base of the soil column; ORCHILEAK does not explicitly represent a groundwater reservoir  
203 and so this imitates the hydrological coupling of swamps and rivers through the groundwater  
204 table. The maximal proportions of each grid which can be covered by floodplains and swamps  
205 are prescribed by the maximal fraction of floodplains (MFF) and the maximal fraction of  
206 swamps (MFS) forcing files respectively (Guimberteau et al., 2012). See also Lauerwald et al.  
207 (2017) and Hastie et al. (2019) for further details. We created an MFF forcing file for the Congo  
208 basin, derived from the Global Wetlands<sup>v3</sup> database; the 232 m resolution tropical wetland map  
209 of Gumbricht et al. (2017) (Fig. 3 a and b). We firstly amalgamated all the categories of wetland  
210 (which include floodplains and swamps) before aggregating them to a resolution of 0.5° (the  
211 resolution at which the floodplain/swamp forcing files are read by ORCHILEAK), assuming  
212 that this represents the maximum extent of inundation in the basin. This results in a mean MFF  
213 of 10%, i.e. a maximum of 10% of the surface area of the Congo basin can be inundated with  
214 water. This is identical to the mean MFF value of 10% produced with the Global Lakes and  
215 Wetlands Database, GLWD (Lehner, & Döll, P.,2004; Borges et al., 2015<sup>b</sup>). We also created  
216 an MFS forcing file from the same dataset (Fig. 3 c and d), merging the ‘swamps’ and ‘fens’  
217 wetland categories (although note that there are virtually no fens in the Congo basin) from  
218 Global Wetlands<sup>v3</sup> database (Gumbricht et al., 2017) and again aggregating them to a 0.5°  
219 resolution. Please see Table 1 of Gumbricht et al. (2017) for further details.

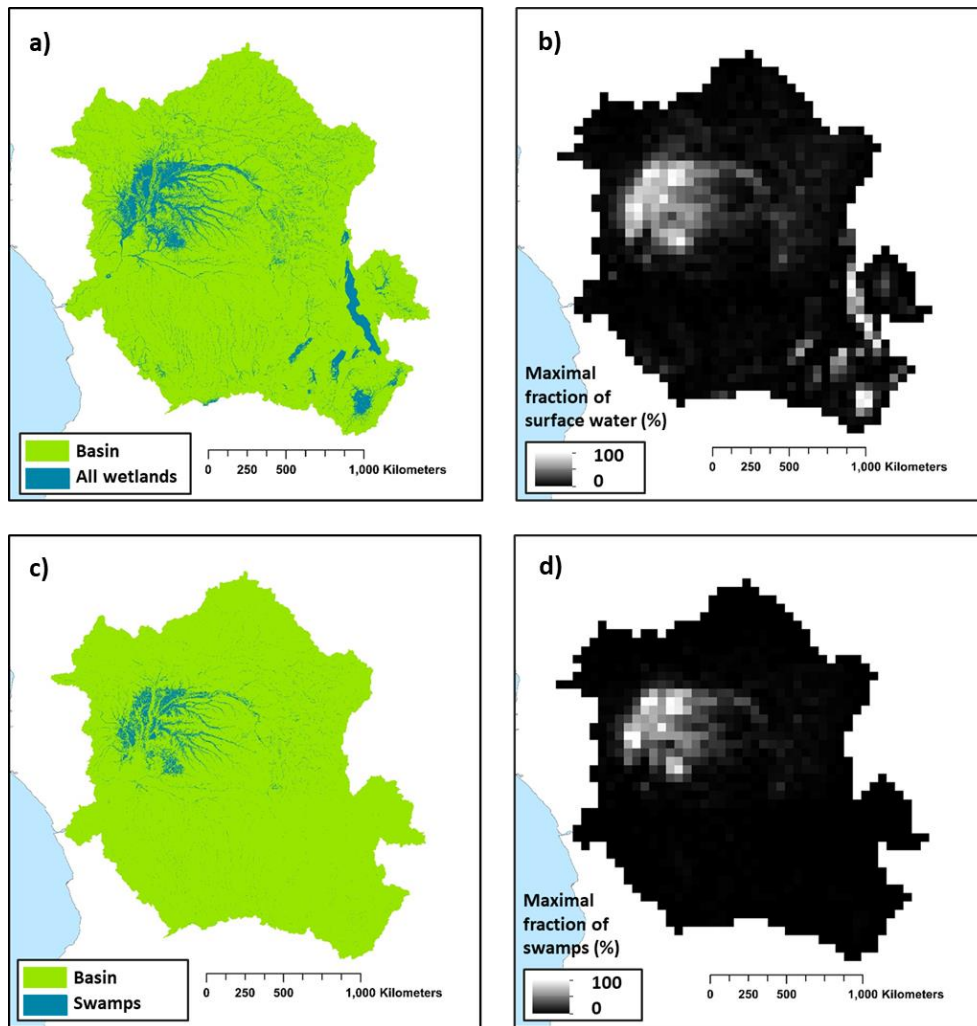


Figure 3: a) Wetland extent (from Gumbricht et al., 2017). b) The new maximal fraction of floodplain (MFF) forcing file developed from a). c) Swamps (including fens) category within Congo basin from Gumbricht et al (2017). d) the new maximal fraction of swamps (MFS) forcing file developed from c). Panels a) and b) are at the same resolution as the Gumbricht dataset (232m) while b) and d) are at a resolution of 0.5°. Note that 0.5° is the resolution of the sub unit basins in ORCHILEAK (Lauerwald et al., 2015), with each 1° grid containing four sub basins.

220

### 221 2.3 Calibration of hydrology

222 As the main driver of the export of C from the terrestrial to aquatic system, it is crucial that the  
 223 model can represent present-day hydrological dynamics, at the very least on the main stem of  
 224 the Congo. As this study is primarily concerned with decadal- centennial timescales our priority  
 225 was to ensure that the model can accurately recreate observed mean annual discharge at the  
 226 most downstream gauging station Brazzaville. We also tested the model's ability to simulate

227 observed discharge seasonality, as well as flood dynamics. Moreover, no data is available with  
228 which to directly evaluate the simulation of DOC and CO<sub>2</sub> leaching from the soil to the river  
229 network, and thus we tested the model's ability to recreate the spatial variation of observed  
230 riverine DOC concentrations and pCO<sub>2</sub> at specific stations where measurements are available  
231 (Borges et al., 2015<sup>b</sup>; Bouillon et al., 2012 & 2014, locations shown in Fig. 1), river DOC and  
232 CO<sub>2</sub> concentration being regarded as an integrator of the C transport at the terrestrial-aquatic  
233 interface.

234 We first ran the model for the present-day period, defined as from 1990 to 2005/2010  
235 depending on which climate forcing data was applied, using four climate forcing datasets;  
236 namely ISIMIP2b (Frieler et al., 2017), Princeton GPCP (Sheffield et al., 2006), GSWP3 (Kim,  
237 2017) and CRUNCEP (Viovy, 2018). We used ISIMIP2b for the historical and future  
238 simulations as it is the only climate forcing dataset to cover the full period (1861-2099).  
239 However, we compared it to other climate forcing datasets for the present day in order to gauge  
240 its ability to simulate observed discharge on the Congo River at Brazzaville (Table A1).  
241 Without calibration, the majority of the different climate forcing model runs performed poorly,  
242 unable to accurately represent the seasonality and mean monthly discharge at Brazzaville  
243 (Table A1). The best performing climate forcing dataset was ISIMIP2b followed by Princeton  
244 GPCP with root mean square errors (RMSE) of 29% and 40% and Nash Sutcliffe efficiencies  
245 (NSE) of 0.20 and -0.25, respectively. NSE is a statistical coefficient specifically used to test  
246 the predictive skill of hydrological models (Nash & Sutcliffe, 1970).

247 For ISIMIP2b we further calibrated key hydrological model parameters, namely the constants  
248 (tau,  $\tau$ ) which ~~determine~~ help to control the water residence time of the groundwater (=slow  
249 reservoir), headwaters (= fast reservoir) and floodplain reservoirs in order to improve the  
250 simulation of observed discharge at Brazzaville and Oubangui (Table 2). To do so, we tested  
251 different combinations of  $\tau$  values ~~water residence times~~ for the three reservoirs, eventually

252 settling on 1, 0.5 and 0.5 (days) for the slow, fast and floodplain reservoirs respectively, all  
253 three being reduced compared to those values used in the original ORCHILEAK calibration  
254 for the Amazon (Lauerwald et al., 2017). The actual residence time of each reservoir is  
255 calculated at each time step. The residence time of the flooded reservoir for example, is a  
256 product of  $\tau_{\text{flood}}$ , a topographical index and the flooded fraction of the grid cell.

257 In order to calibrate the simulated discharge against observations, we first modified the flood  
258 dynamics of ORCHILEAK in the Congo Basin for the present day by adjusting bank-full  
259 discharge ( $\text{streamr}_{50\text{th}}$ , Lauerwald et al., 2017) and 95<sup>th</sup> percentile of water level heights  
260 ( $\text{floodh}_{95\text{th}}$ ). As in previous studies on the Amazon basin (Lauerwald et al. 2017, Hastie et al.,  
261 2019) we defined bank-full discharge, i.e. the threshold discharge at which floodplain  
262 inundation starts (i.e. overtopping of banks), as the median discharge (50<sup>th</sup> percentile i.e.  
263  $\text{streamr}_{50\text{th}}$ ) of the present-day climate forcing period (1990 to 2005). After re-running each  
264 model parametrization (different  ~~$\tau$  values~~~~water residence times~~) to obtain those bank-full  
265 discharge values, we calculated  $\text{floodh}_{95\text{th}}$  over the simulation period for each grid cell (Table  
266 1). This value is assumed to represent the water level over the river banks at which the  
267 maximum horizontal extent of floodplain inundation is reached. We then ran the model for a  
268 final time and validated the outputs against discharge data at Brazzaville (Cochonneau et al.,  
269 2006, Fig. 1). This procedure was repeated iteratively with the ISIMIP2b climate forcing,  
270 modifying the  ~~$\tau$  values~~~~water residence times~~ of each reservoir in order to find the best  
271 performing parametrization.

272 We firstly compared simulated versus observed discharge at Brazzaville (NSE, RMSE, Table  
273 2), before using the data of Bouillon et al. (2014) to further validate discharge at Bangui (Fig.  
274 1) on the main tributary Oubangui. In addition, we compared the simulated seasonality of  
275 flooded area against the satellite derived dataset GIEMS (Prigent et al., 2007; Becker et al.,  
276 2018), within the Cuvette Centrale wetlands (Fig. 1).



## 277 **2.4 Simulation set-up**

278 A list of the main forcing files used, along with data sources, is presented in Table 1. The  
279 derivation of the floodplains and swamp (MFF & MFS) is described in section 2.2 while the  
280 calculation of “bankfull discharge” ( $\text{streamr}_{50\text{th}}$ ) and “95th percentile of water table height over  
281 flood plain” ( $\text{floodh}_{95\text{th}}$ ) (Table 1) is described in section 2.3.

### 282 **2.4.1 Soil carbon spin up**

283 ORCHILEAK includes a soil module, primarily derived from ORCHIDEE-SOM (Camino  
284 Serrano, 2018). The soil module has 3 different pools of soil DOC; the passive, slow and active  
285 pool and these are defined by their source material and residence times ( $\tau_{\text{carbon}}$ ). ORCHILEAK  
286 also differentiates between flooded and non-flooded soils; decomposition rates of DOC, SOC  
287 and litter being reduced (3 times lower) in flooded soils. In order for the soil C pools to reach  
288 steady state, we spun-up the model for around 9,000 years, with fixed land-use representative  
289 of 1861, and looping over the first 30 years of the ISMSIP2b climate forcing data (1861-1890).  
290 During the first 2,000 years of spin-up, we ran the model with an atmospheric  $\text{CO}_2$   
291 concentration of  $350 \mu\text{atm}$  and default soil C residence times ( $\tau_{\text{carbon}}$ ) halved, which allowed it  
292 to approach steady-state more rapidly. Following this, we ran the model for a further 7,000  
293 years reverting to the default  $\tau_{\text{carbon}}$  values. At the end of this process, the soil C pools had  
294 reached approximately steady state;  $<0.02\%$  change in each pool over the final century of the  
295 spin-up.

### 296 **2.4.2 Transient simulations**

297 After the spin-up, we ran a historical simulation from 1861 until the present day, 2005 in the  
298 case of the ISIMIP2b climate forcing data. We then ran a future simulation until 2099, using  
299 the final year of the historical simulation as a restart file. In both of these simulations, climate,  
300 atmospheric  $\text{CO}_2$  and land-cover change were prescribed as fully transient forcings according  
301 to the RCP6.0 scenario. For climate variables, we used the IPSL-CM5A-LR model outputs for

302 RCP 6.0, bias corrected by the ISIMIP2b procedure (Frieler et al., 2017; Lange et al., 2017),  
303 while land-use change was taken from the 5th Coupled Model Intercomparison Project  
304 (CMIP5). As our aim is to investigate long-term trends, we calculated 30-years running means  
305 of simulated C flux outputs in order to smooth interannual variations. RCP 6.0 is an emissions  
306 pathway that leads to a “stabilization of radiative forcing at 6.0 Watts per square meter ( $\text{Wm}^{-2}$ )  
307 in the year 2100 without exceeding that value in prior years” (Masui et al., 2011). It is  
308 characterised by intermediate energy intensity, substantial population growth, mid-high C  
309 emissions, increasing cropland area to 2100 and decreasing natural grassland area (van Vuuren  
310 et al., 2011). In the paper which describes the development of the future land use change  
311 scenarios under RCP 6.0 (Hurtt et al., 2011), it is shown that land use change is highly sensitive  
312 to land use model assumptions, such as whether or not shifting cultivation is included. The  
313 LUH1 reconstruction for instance indicates shifting cultivation affecting all of the tropics with  
314 a residence time of agriculture of 15 years, whereas the review from Heinemann et al. (2017)  
315 revised downwards the area of this type of agriculture, with generally low values in Congo,  
316 except in the North East and South East, but suggested a shorter turnover of agriculture of two  
317 years only. In view of such uncertainties, we did not include shifting agriculture in the model.  
318 Moreover, there is considerable uncertainty associated with the effect of future land-use change  
319 in Africa (Hurtt et al., 2011). We chose RCP 6.0 as it represents a no mitigation (mid-high  
320 emissions) scenario. Moreover, the ISIMIP2b data only provided two RCPs at the time we  
321 performed the simulations; RCP 2.6 (low emission) and RCP 6.0.

322 With the purpose of evaluating separately the effects of land-use change, climate change, and  
323 rising atmospheric  $\text{CO}_2$ , we ran a series of factorial simulations. In each simulation, one of  
324 these factors was fixed at its 1861 level (the first year of the simulation), or in the case of fixed  
325 climate change, we looped over the years 1861-1890. The outputs of these simulations (also  
326 30-year running means) were then subtracted from the outputs of the main simulation (original

327 run with all factors varied) so that we could determine the contribution of each driver (Fig. 10,  
 328 Table 1).

<b>Variable</b>	<b>Spatial resolution</b>	<b>Temporal resolution</b>	<b>Data source</b>
Rainfall, <del>snowfall</del> , incoming shortwave and longwave radiation, air temperature, relative humidity and air pressure (close to surface), wind speed (10 m above surface)	1°	1 day	ISIMIP2b, IPSL-CM5A-LR model outputs for RCP6.0 (Frieler et al., 2017)
Land cover (and change)	0.5°	annual	LUH-CMIP5
Poor soils	0.5°	annual	Derived from HWSO v 1.1 (FAO/IIASA/ISRIC/ISS-CAS/JRC, 2009)
Stream flow directions	0.5°	annual	STN-30p (Vörösmarty et al., 2000)
Floodplains and swamps fraction in each grid (MFF & MFS)	0.5°	annual	derived from the wetland high resolution data of Gumbrecht et al. (2017)
River surface areas	0.5°	annual	Lauerwald et al. (2015)
Bankfull discharge (streamr <sub>50th</sub> )	1°	annual	derived from calibration with ORCHILEAK (see section 2.3)
95th percentile of water table height over flood plain (floodh <sub>95th</sub> )	1°	annual	derived from calibration with ORCHILEAK (see section 2.3)

## 329 **2.5 Evaluation and analysis of simulated fluvial C fluxes**

330 We first evaluated DOC concentrations and  $p\text{CO}_2$  at several locations along the Congo  
 331 mainstem (Fig. 1), and on the Oubangui river against the data of Borges et al. (2015<sup>b</sup>) and  
 332 Bouillon et al. (2012, 2014) We also compared the various simulated components of the net C  
 333 balance (e.g. NPP) of the Congo against values described in the literature (Williams et al.,  
 334 2007; Lewis et al., 2009; Verhegghen et al., 2012; Valentini et al., 2014; Yin et al., 2017). In  
 335 addition, we assessed the relationship between the interannual variation in present day (1981-  
 336 2010) C fluxes of the Congo basin and variation in temperature and rainfall. This was done  
 337 through linear regression using STATISTICA<sup>TM</sup>. We found trends in several of the fluxes over  
 338 the 30-year period (1981-2010) and thus detrended the time series with the “Detrend” function,  
 339 part of the “SpecsVerification” package in R (R Core Team 2013), before undertaking the  
 340 statistical analysis focused on the climate drivers of inter-annual variability.

## 341 **2.6 Calculating the net carbon balance of the Congo basin**

342 We calculated Net Ecosystem Production (NEP) by summing the terrestrial and aquatic C  
343 fluxes of the Congo basin (Eq. 1), while we incorporated disturbance fluxes (Land-use change  
344 flux and harvest flux) to calculate Net Biome Production (NBP) (Eq. 2). Positive values of  
345 NBP and NEP equate to a net terrestrial C sink.

346 NEP is defined as follows:

$$347 \quad \left. \begin{array}{l} \text{NEP} = \text{NPP} + \text{TF} - \text{SHR} - \text{FCO}_2 - \text{LE}_{\text{Aquatic}} \end{array} \right\} \quad (1)$$

348 Where *NPP* is terrestrial net primary production, *TF* is the throughfall flux of DOC from the  
349 canopy to the ground, *SHR* is soil heterotrophic respiration (only that evading from the *terra-*  
350 *firme* soil surface); *FCO<sub>2</sub>* is CO<sub>2</sub> evasion from the water surface and *LE<sub>Aquatic</sub>* is the lateral  
351 export flux of C (DOC + dissolved CO<sub>2</sub>) to the coast. NBP is equal to NEP except with the  
352 inclusion of the C lost (or possibly gained) via land use change (*LUC*) and crop harvest (*HAR*).  
353 Wood harvest is not included for logging and forestry practices, but during deforestation LUC,  
354 a fraction of the forest biomass is harvested and channelled to wood product pools with  
355 different decay constants. *LUC* includes land conversion fluxes and the lateral export of wood  
356 products biomass, that is, assuming that wood products from deforestation are not consumed  
357 and released as CO<sub>2</sub> over the Congo, but in other regions:

$$358 \quad \text{NBP} = \text{NEP} - (\text{LUC} + \text{HAR}) \quad (2)$$

359

## 360 **3. Results**

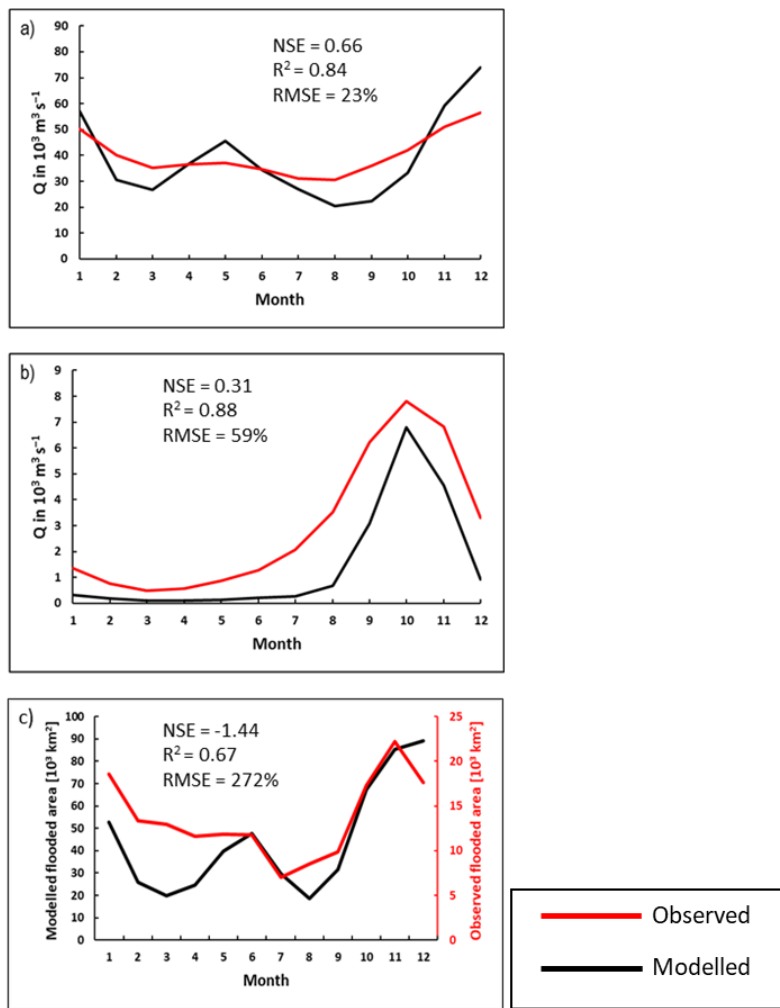
### 361 **3.1 Simulation of hydrology and aquatic carbon fluxes**

362 The final model configuration is able to closely reproduce the mean monthly discharge at  
363 Brazzaville (Fig. 4 a), Table 2) and captures the seasonality moderately well (Fig. 4 a, Table 2,

364 RMSE =23%,  $R^2$  =0.84 versus RMSE= 29% and  $R^2$  =0.23 without calibration, Table A1). At  
365 Bangui on the Oubangui River (Fig. 1), the model is able to closely recreate observed  
366 seasonality (Fig. 4 b), RMSE =59%,  $R^2$  =0.88) but substantially underestimates the mean  
367 monthly discharge, our value being only 50% of the observed. We produce reasonable NSE  
368 values of 0.66 and 0.31 for Brazzaville and Bangui respectively, indicating that the model is  
369 moderately accurate in its simulation of seasonality.

370 We also evaluated the simulated seasonal change in flooded area in the central (approx.  
371 200,000 km<sup>2</sup>, Fig. 1) part of the Cuvette Centrale wetlands against the GIEMS inundation  
372 dataset (1993-2007, maximum inundation minus minimum or permanent water bodies, Prigent  
373 et al., 2007; Becker et al., 2018). While our model is able to represent the seasonality in flooded  
374 area relatively well ( $R^2$  =0.75 Fig. 4 c), it considerably overestimates the magnitude of flooded  
375 area relative to GIEMS (Fig. 4 c, Table 2). However, the dataset that we used to define the  
376 MFF and MFS forcing files (Gumbricht et al., 2017) is produced at a higher resolution than  
377 GIEMS and will capture smaller wetlands than the GIEMS dataset, and thus the greater flooded  
378 area is to be expected. GIEMS is also known to underestimate inundation under vegetated areas  
379 (Prigent et al., 2007; Papa et al., 2010) and has difficulties to capture small inundated areas  
380 (Prigent et al., 2007; Lauerwald et al., 2017). Indeed, with the GIEMS data we produce an  
381 overall flooded area for the Congo Basin of just 3%, less than one-third of that produced with  
382 the Gumbricht dataset (Gumbricht et al., 2017) or the GLWD (Lehner, & Döll, P.,2004). As  
383 such, it is to be expected that there is a large RMSE (272%, Table 2) between simulated flooded  
384 area and GIEMS; more importantly, the seasonality of the two is highly correlated ( $R^2$  = 0.67,  
385 Table 2).

386



387

388 **Figure 4: Seasonality of simulated versus observed discharge at a) Brazzaville on the**  
389 **Congo (Cochonneau et al., 2006), b) Bangui on the Oubangui (Bouillon et al., 2014) 1990-**  
390 **2005 monthly mean and c) flooded area in the central (approx. 200,000 km<sup>2</sup>) area of the**  
391 **Cuvette Centrale wetlands versus GIEMS (1993-2007, Becker et al., 2018). The observed**  
**flooded area data represents the maximum minus minimum (permanent water bodies**  
**such as rivers) GIEMS inundation. See Figure 1 for locations.**

391

**Table 2: Performance statistics for modelled versus observed seasonality of discharge and flooded area in Cuvette Centrale. Observed flooded area is from GIEMS (Papa et al., 2010, Becker et al., 2018).**

Station	RSME	NSE	R <sup>2</sup>	Simulated mean monthly discharge (m <sup>3</sup> s <sup>-1</sup> )	Observed -mean monthly discharge (m <sup>3</sup> s <sup>-1</sup> )
Brazzaville	23%	0.66	0.84	38,944	40,080
Bangui	59%	0.31	0.88	1,448	2,923
				Simulated mean monthly flooded area (10 <sup>3</sup> km <sup>2</sup> )	Observed mean monthly flooded area (10 <sup>3</sup> km <sup>2</sup> )
Flooded area (Cuvette Centrale)	272%	-1.44	0.67	44	14

392

393 In Figure 5, we compare simulated DOC concentrations at six locations (Fig. 1) along the  
394 Congo River and Oubangui tributary, against the observations of Borges et al. (2015<sup>b</sup>). We  
395 show that we can recreate the spatial variation in DOC concentration within the Congo basin  
396 relatively closely with an R<sup>2</sup> of 0.74 and an RMSE of 24% (Fig. 5). We are also able to  
397 simulate the broad spatial pattern of pCO<sub>2</sub> measured in the main-stem Congo reported by  
398 Borges et al. (2019). During high flow season (mean of 6 consecutive months of highest flow,  
399 2009-2019 to account for interannual variation) we simulate a mean pCO<sub>2</sub> of 3,373 ppm and  
400 5,095 ppm at Kisangani and Kinshasa (Brazzaville) respectively, compared to the observed  
401 values of 2,424 ppm and 5,343 ppm during high water (measured in December 2013, Borges  
402 et al., 2019) (Table 3). Similarly, during low flow season (mean of 6 consecutive months of  
403 lowest flow, 2009-2019) we simulate a mean pCO<sub>2</sub> of 1,563 ppm and 2,782 ppm at Kisangani  
404 and Kinshasa respectively, compared to the observed values of 1,670 ppm and 2,896 ppm  
405 during falling water (June 2014, Borges et al., 2019) (Table 3).



406

407 While we are able to recreate observed spatial differences in DOC and  $p\text{CO}_2$ , as well as broad  
408 seasonal variations, we are not able to correctly predict the exact timing of the simulated  
409 highs and lows, a reflection of not fully capturing the hydrological seasonality. For example,  
410 our mean June  $p\text{CO}_2$  at Kinshasa (Brazzaville) is 4,470 ppm, while Borges et al measured a  
411 mean of 2,896 ppm (Table 3). However, our value for July of 2,621 ppm is much closer, and  
412 moreover our mean value for December of 5,154 ppm is relatively close to the observed  
413 value of 5,343 ppm. Similarly, we fail to predict the timing of the June falling water at  
414 Kisangani (Table 3).

415 In Figure 6, we compare simulated  $p\text{CO}_2$  against the observed monthly time series at Bangui  
416 on the Oubangui River (Bouillon et al., 2012 & 2014), as far as we are aware the longestmost  
417 complete time series of  $p\text{CO}_2$  published (and accessible) from the Congo basin, spanning  
418 March 2010 to March 2012 (with only the single month of June 2010 missing). Again, while  
419 the model fails to correctly predict the precise timing of the peak as with the Kinshasa and  
420 Kisangani datasets the broad seasonal variation in  $p\text{CO}_2$  is captured, with the observed and  
421 modelled times series ranging from 227- 4040 ppm and 415- 2928 ppm, respectively (Fig. 6).

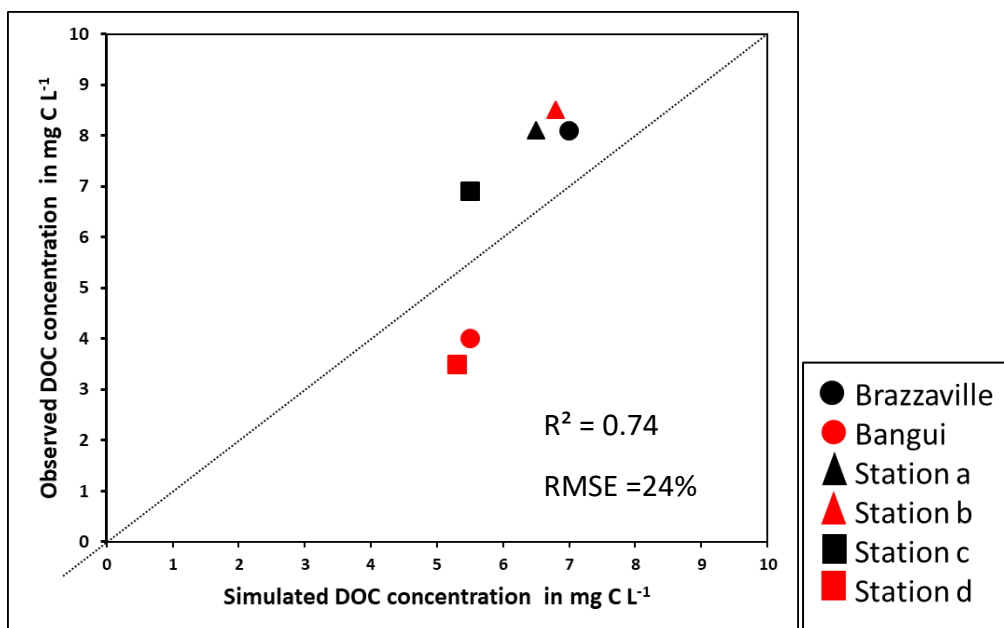
422

423

424

425

426



427

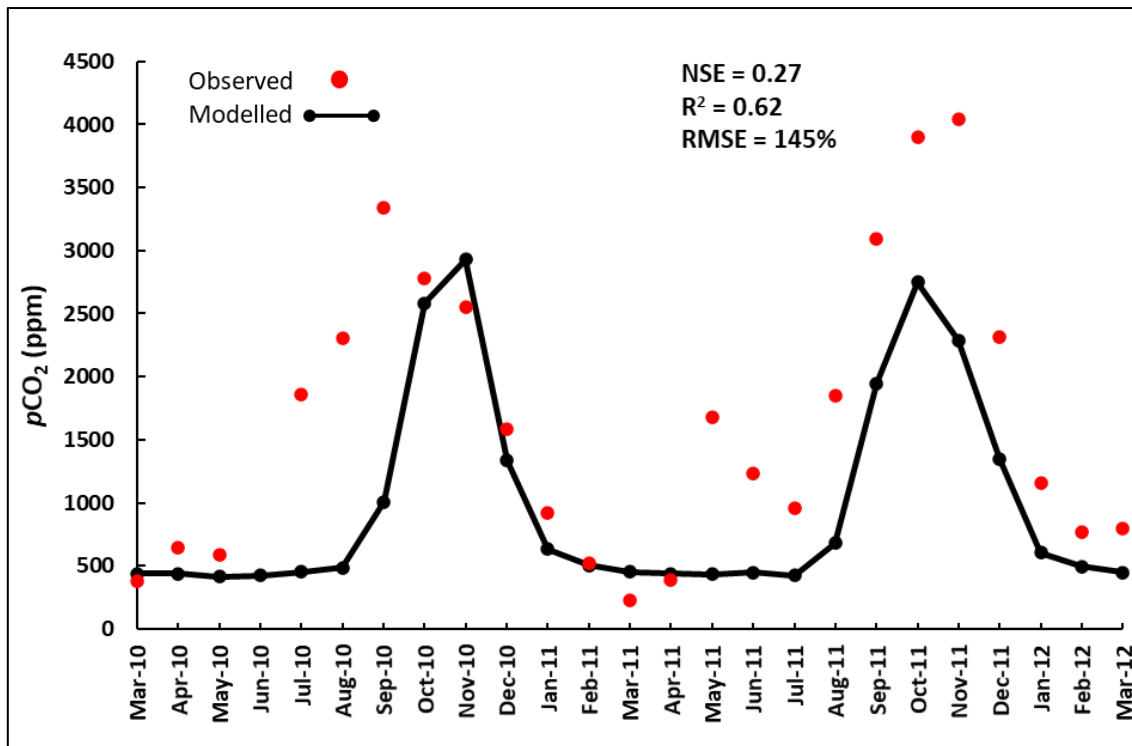
**Figure 5: Observed (Borges et al., 2015<sup>a</sup>) versus simulated DOC concentrations at several sites along the Congo and Oubangui rivers. See Fig. 1 for locations. The simulated and observed DOC concentrations represent the median values across the particular sampling period at each location detailed in Borges et al. (2015<sup>a</sup>).**

428

**Table 3: Observed (Borges et al., 2019) and modelled  $p\text{CO}_2$  (in ppm) at Kinshasa (Brazzaville) and Kisangani on the Congo river at various water levels.**

Location	Observed $p\text{CO}_2$ highwater (December 2013)	Modelled $p\text{CO}_2$ highwater (December Mean 2009-2019)	Modelled $p\text{CO}_2$ high flow season (mean of 6 consecutive months of highest flow 2009-2019)	Observed $p\text{CO}_2$ falling water (June 2014)	Modelled $p\text{CO}_2$ falling water (June mean 2009-2019)	Modelled $p\text{CO}_2$ low flow season (mean of 6 consecutive months of lowest flow 2009-2019)
Kinshasa (Brazzaville)	5,343	5,154	5,095	2,896	4,470	2,782
Kisangani	2,424	2,166	3,373	1,670	3,126	1,563

429



431

432

**Figure 6: Time series of observed versus simulated  $p\text{CO}_2$  at Bangui on the River Oubangui. Observed data is from Bouillon et al., 2012 and Bouillon et al., 2014.**

433

### 434 3.2 Carbon fluxes along the Congo basin for the present day

435 For the present day (1981-2010) we estimate a mean annual terrestrial net primary production

436 (NPP) of  $5,800 \pm 166$  (standard deviation, SD)  $\text{Tg C yr}^{-1}$  (Fig. 7), corresponding to a mean areal

437 C fixation rate of approximately  $1,500 \text{ g C m}^{-2} \text{ yr}^{-1}$  (Fig. 8 a). We find a significant positive

438 correlation between the interannual variation of NPP and rainfall (detrended  $R^2 = 0.41$ ,  $p < 0.001$ ,

439 Table A2) and a negative correlation between annual NPP and temperature (detrended  $R^2 =$

440  $0.32$ ,  $p < 0.01$ , Table A2). We also see considerable spatial variation in NPP across the Congo

441 Basin (Fig.8 a).

442 We simulate a mean soil heterotrophic respiration (SHR) of  $5,300 \pm 99 \text{ Tg C yr}^{-1}$  across the

443 Congo basin (Fig. 7). Contrary to NPP, interannual variation in annual SHR is positively

444 correlated with temperature (detrended  $R^2=0.57$ ,  $p<0.0001$ , Table A2) and inversely correlated  
445 with rainfall (detrended  $R^2=0.10$ ), though the latter relationship is not significant ( $p>0.05$ ).  
446 We estimate a mean annual aquatic  $\text{CO}_2$  evasion rate of  $1,363 \pm 83 \text{ g C m}^{-2} \text{ yr}^{-1}$ , amounting to  
447 a total of  $235 \pm 54 \text{ Tg C yr}^{-1}$  across the total water surfaces of the Congo basin (Fig. 7) and  
448 attribute 85% of this flux to flooded areas, meaning that only  $32 \text{ Tg C yr}^{-1}$  is evaded directly  
449 from the river surface. Interannual variation in aquatic  $\text{CO}_2$  evasion (1981-2010) shows a  
450 strong positive correlation with rainfall (detrended  $R^2=0.75$ ,  $p<0.0001$ , Table A2) and a weak  
451 negative correlation with temperature (detrended  $R^2=0.09$ , not significant,  $p>0.05$ ). Aquatic  
452  $\text{CO}_2$  evasion also exhibits substantial spatial variation (Fig.8, d), displaying a similar pattern to  
453 both terrestrial DOC leaching ( $\text{DOC}_{\text{inp}}$ ) ( $R^2=0.81$ ,  $p<0.0001$ , Fig.8, b) as well as terrestrial  
454  $\text{CO}_2$  leaching ( $\text{CO}_{2\text{inp}}$ ) ( $R^2=0.96$ ,  $p<0.0001$ , Fig.8, c) into the aquatic system, but not terrestrial  
455 NPP ( $R^2=0.01$ ,  $p<0.05$ , Fig.8, a). We simulate a mean annual flux of DOC throughfall from  
456 the canopy of  $27 \pm 1 \text{ Tg C yr}^{-1}$  and C (DOC + dissolved  $\text{CO}_2$ ) export flux to the coast of  $15 \pm 4$   
457  $\text{Tg C yr}^{-1}$  (Fig. 7).

458 For the present day (1981-2010) we estimate a mean annual net ecosystem production (NEP)  
459 of  $277 \pm 137 \text{ Tg C yr}^{-1}$  and a net biome production (NBP) of  $107 \pm 133 \text{ Tg C yr}^{-1}$  (Fig. 7).  
460 Interannually, both NEP and NBP exhibit a strong inverse correlation with temperature  
461 (detrended NEP  $R^2=0.55$ ,  $p<0.0001$ , detrended NBP  $R^2=0.54$ ,  $p<0.0001$ ) and weak positive  
462 relationship with rainfall (detrended NEP  $R^2=0.16$ ,  $p<0.05$ , detrended NBP  $R^2=0.14$ ,  $p<0.05$ ).  
463 Furthermore, we simulate a present day (1981-2010) living biomass of  $41 \pm 1 \text{ Pg C}$  and a total  
464 soil C stock of  $109 \pm 1 \text{ Pg C}$ .

465

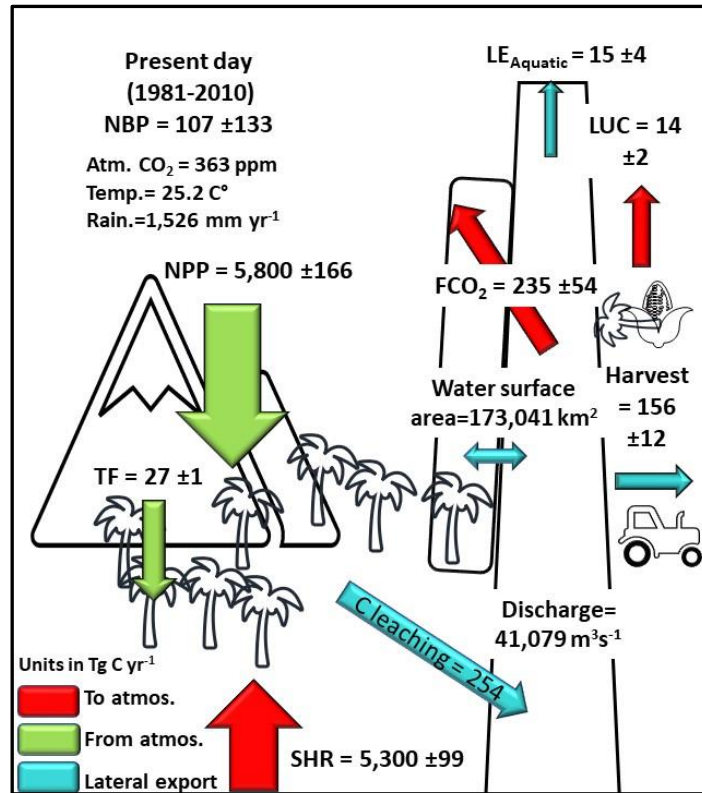
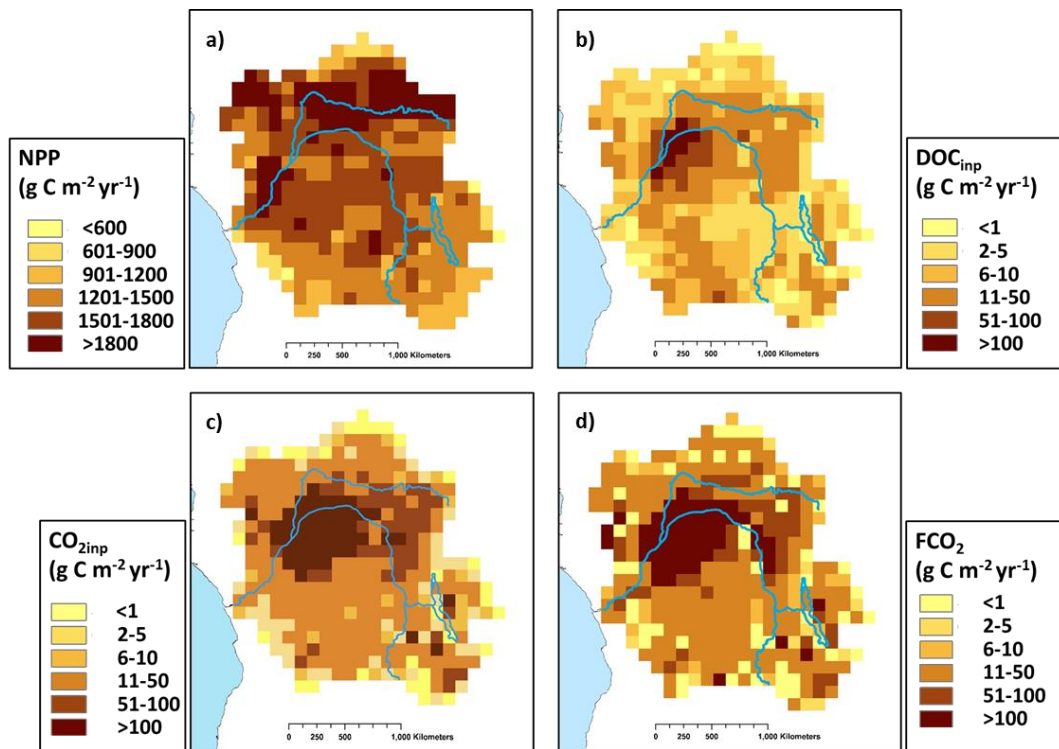


**Figure 7: Annual C budget (NBP) for the Congo basin for the present day (1981-2010) simulated with ORCHILEAK, where NPP is terrestrial net primary productivity, TF is throughfall, SHR is soil heterotrophic respiration, FCO<sub>2</sub> is aquatic CO<sub>2</sub> evasion, LOAC is C leakage to the land-ocean aquatic continuum (FCO<sub>2</sub> + LE<sub>Aquatic</sub>), LUC is flux from Land-use change, and LE<sub>Aquatic</sub> is the export C flux to the coast. Range represents the standard deviation (SD) from 1981-2010.**



467

Figure 8: Present day (1981-2010) spatial distribution of a) terrestrial net primary productivity (NPP), b) dissolved organic carbon export from soils and floodplain vegetation into the aquatic system (DOC<sub>inp</sub>), c) CO<sub>2</sub> leaching from soils and floodplain vegetation into the aquatic system (CO<sub>2inp</sub>)- and d) aquatic CO<sub>2</sub> evasion (FCO<sub>2</sub>). Main rivers in blue. All at a resolution of 1°

468

### 469 3.3 Long-term temporal trends in carbon fluxes

470 We find an increasing trend in aquatic CO<sub>2</sub> evasion (Fig. 9 a) throughout the simulation period,  
 471 rising slowly at first until the 1960s when the rate of increase accelerates. In total CO<sub>2</sub> evasion  
 472 rose by 79% from 186 Tg C yr<sup>-1</sup> at the start of the simulation (1861-1890 mean) (Fig. 10) to  
 473 333 Tg C yr<sup>-1</sup> at the end of this century (2070-2099 mean, Fig. 10), while the increase until the  
 474 present day (1981-2010 mean) is ~~is~~ +26 % (to 235 Tg C yr<sup>-1</sup>), though these trends are not  
 475 uniform across the basin (Fig A1). The lateral export flux of C to the coast (LE<sub>Aquatic</sub>) follows  
 476 a similar relative change (Fig. 9b), rising by 67% in total, from 12 Tg C yr<sup>-1</sup> (Fig. 10) to 15 Tg  
 477 C yr<sup>-1</sup> for the present day, and finally to 20 Tg C yr<sup>-1</sup> (2070-2099 mean, Fig. 10). This is greater

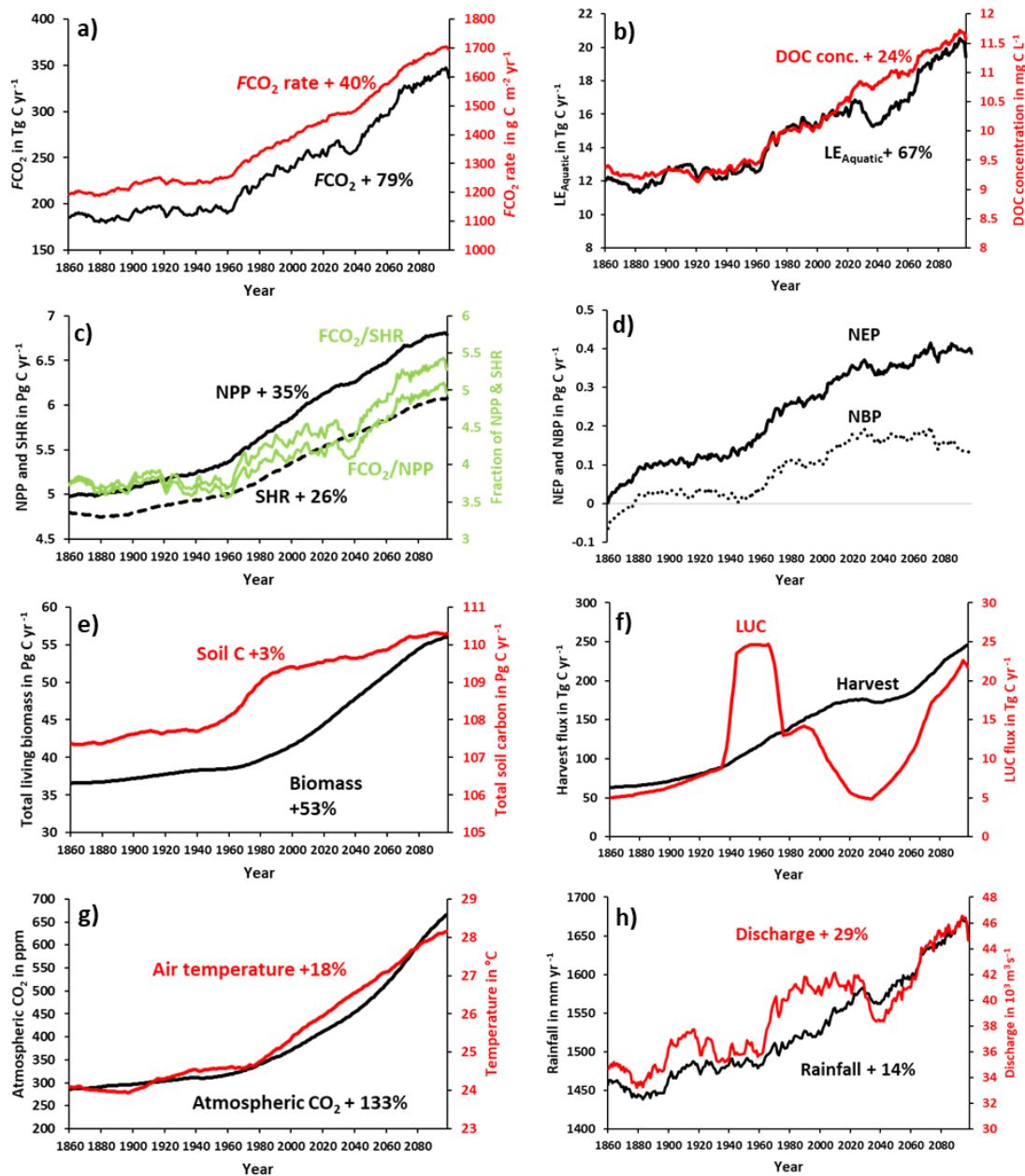
478 than the equivalent increase in DOC concentration (24%, Fig. 9b) due to the concurrent rise in  
479 rainfall (by 14%, Fig 9h) and in turn discharge (by 29%, Fig. 9h).

480 Terrestrial NPP and SHR also exhibit substantial increases of 35% and 26% respectively across  
481 the simulation period and similarly rise rapidly after 1960 (Fig. 9c). NEP, NBP (Fig. 9d) and  
482 living biomass (Fig. 9 e) follow roughly the same trend as NPP, but NEP and NBP begin to  
483 slow down or even level-off around 2030 and in the case of NBP, we actually simulate a  
484 decreasing trend over approximately the final 50 years. Interestingly, the proportion of NPP  
485 lost to the LOAC also increases from approximately 3% to 5% (Fig. 9c). We also find that  
486 living biomass stock increases by a total of 53% from 1861 to 2099. Total soil C also increases  
487 over the simulation but only by 3% from 107 to 110 Pg C yr<sup>-1</sup> (Fig. 9e). Emissions from land-  
488 use change (LUC) show considerable decadal fluctuation increasing rapidly in the second half  
489 of the 20<sup>th</sup> century and decreasing in the mid-21<sup>st</sup> century before rising again towards the end  
490 of the simulation (Fig. 9f). The harvest flux (Fig. 9f) rises throughout the simulation with the  
491 exception of a period in the mid-21<sup>st</sup> century during which it stalls for several decades. This is  
492 reflected in the change in land-use areas from 1861- 2099 (Fig. A2, Table A3) during which  
493 the natural forest and grassland PFTs marginally decrease while both C<sub>3</sub> and C<sub>4</sub> agricultural  
494 grassland PFTs increase.

495

496





498

499

500

501

502

### 503 3.4 Drivers of simulated trends in carbon fluxes

504

505

Figure 9: Simulation results for various C fluxes and stocks from 1861-2099, using IPSL-CM5A-LR model outputs for RCP 6.0 (Frierler et al., 2017). All panels except for atmospheric CO<sub>2</sub>, biomass and soil C correspond to 30-year running means of simulation outputs. This was done in order to suppress interannual variation, as we are interested in longer-term trends.

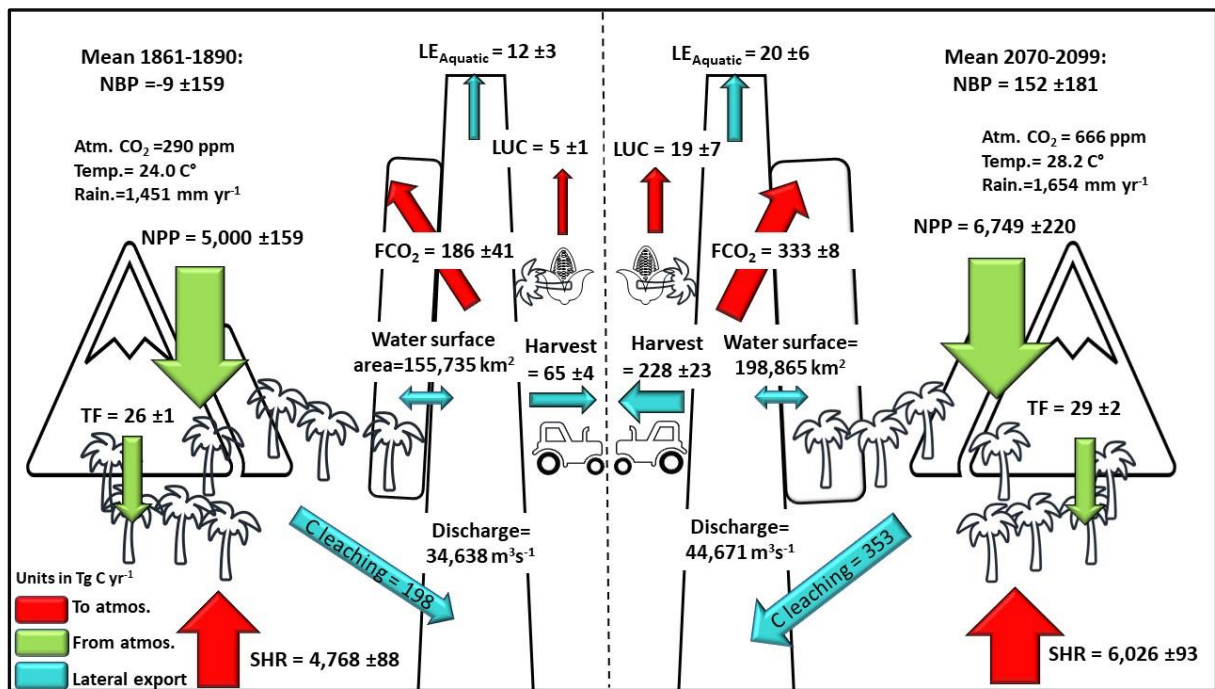
The dramatic increase in the concentration of atmospheric CO<sub>2</sub> (Fig. 9 g) and subsequent fertilization effect on terrestrial NPP has the greatest overall impact on all of the fluxes across

506 the simulation period (Fig. 11). It is responsible for the vast majority of the growth in NPP,  
507 SHR, aquatic CO<sub>2</sub> evasion and flux of C to the coast (Fig. 11 a, b, c & d). The effect of LUC  
508 on these four fluxes is more or less neutral, while the impact of climate change is more varied.  
509 The aquatic fluxes (Fig. 11 c, d) respond positively to an acceleration in the increase of both  
510 rainfall (and in turn discharge, Fig. 9 h) and temperature (Fig. 9 g) starting around 1970. From  
511 around 2020, the impact of climate change on the lateral flux of C to the coast (Fig 11 d) reverts  
512 to being effectively neutral, likely a response to a slowdown in the rise of rainfall and indeed a  
513 decrease in discharge (Fig 9 h), as well as perhaps the effect of temperature crossing a  
514 threshold. The response of the overall loss of terrestrial C to the LOAC (i.e. the ratio of  
515 LOAC/NPP, Fig. 11 e) is relatively similar to the response of the individual aquatic fluxes but  
516 crucially, climate change exerts a much greater impact, contributing substantially to an increase  
517 in the loss of terrestrial NPP to the LOAC in the 1960s, and again in the second half of the 21<sup>st</sup>  
518 century. These changes closely coincide with the pattern of rainfall and in particular with  
519 changes in discharge (Fig. 9 h).

520 Overall temperature and rainfall increase by 18% and 14% from 24°C to 28°C and 1457mm to  
521 1654mm respectively, but in Fig. A2 one can see that this increase is non-uniform across the  
522 basin. Generally speaking, the greatest increase in temperature occurs in the south of the basin  
523 while it is the east that sees the largest rise in rainfall (Fig. A2). Land-use changes are similarly  
524 non-uniform (Fig. A2).

525 The response of NBP and in NEP (Fig.11 f, g) to anthropogenic drivers is more complex. The  
526 simulated decrease in NBP towards the end of the run is influenced by a variety of factors;  
527 LUC and climate begin to have a negative effect on NBP (contributing to a decrease in NBP)  
528 at a similar time while the positive impact (contributing to an increase in NBP) of atmospheric  
529 CO<sub>2</sub> begins to slow down and eventually level-off (Fig.11 g). LUC continues to have a positive  
530 effect on NEP (Fig.11 f) due to the fact that the expanding C<sub>4</sub> crops have a higher NPP than

531 forests, while it has an overall negative effect on NBP at the end of the simulation due to the  
 532 inclusion of emissions from crop harvest.



533

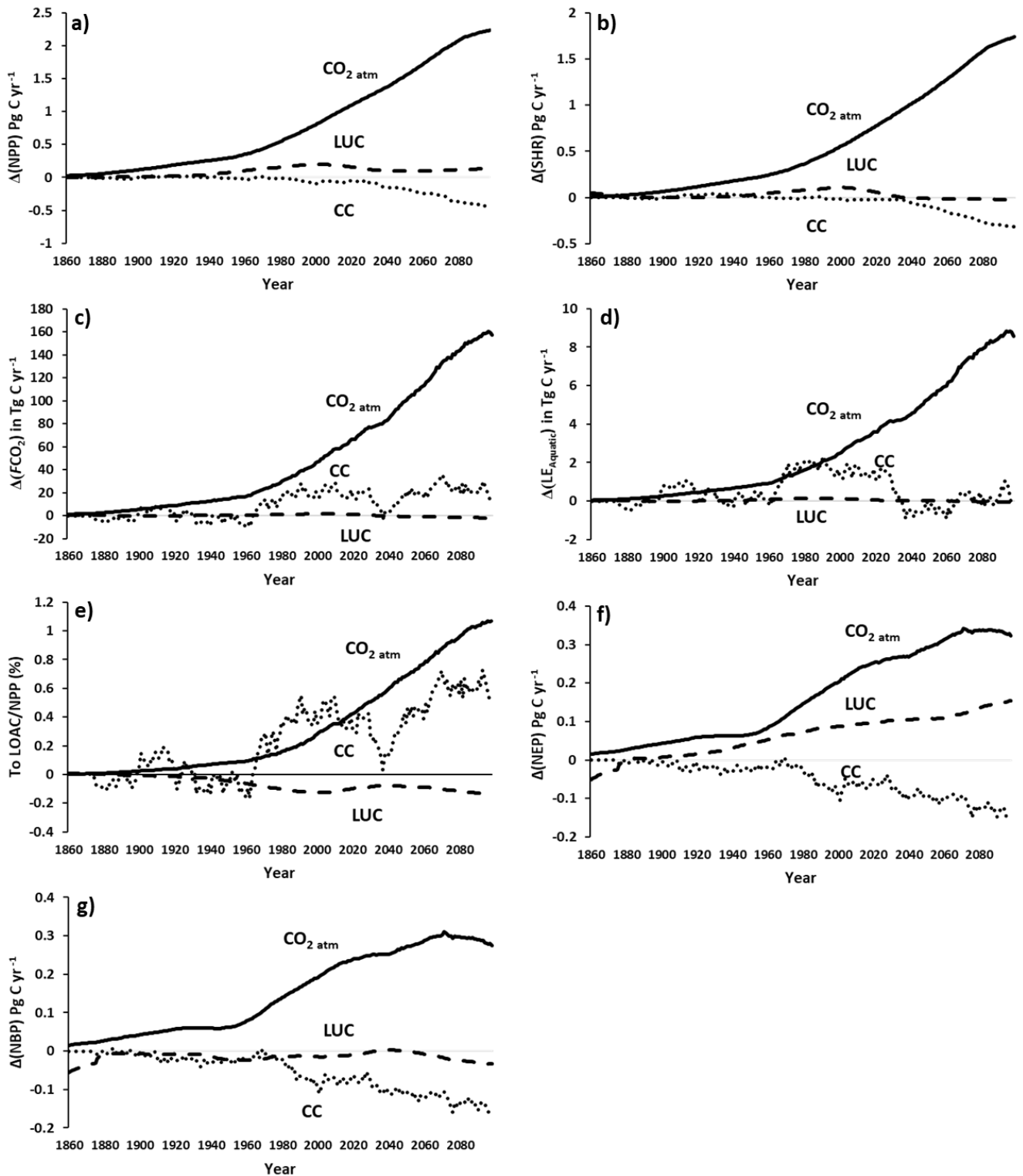
534 **Figure 10: Annual C budget (NBP) for the Congo basin for; left, the Year 1861 and right, the**  
 535 **Year 2099, simulated with ORCHILEAK. NPP is terrestrial net primary productivity, TF is**  
 536 **throughfall, SHR is soil heterotrophic respiration, FCO<sub>2</sub> is aquatic CO<sub>2</sub> evasion, LOAC is C**  
 537 **leakage to the land-ocean aquatic continuum (FCO<sub>2</sub> + LE<sub>Aquatic</sub>), LUC is flux from Land-use**  
 538 **change, and LE<sub>Aquatic</sub> is the export C flux to the coast. Range represents the standard deviation**  
 539 **(SD).**

540

541

542

543



545 **Figure 11: Contribution of anthropogenic drivers; atmospheric CO<sub>2</sub> concentration (CO<sub>2 atm</sub>),**  
 climate change (CC) and land use change (LUC) to changes in the various carbon fluxes along  
 the Congo Basin, under IPSL-CM5A-LR model outputs for RCP 6.0 (Frieler et al., 2017).

## 547 4. Discussion

### 548 4.1 Congo basin carbon balance

549 We simulate a mean present-day terrestrial NPP of approximately  $1,500 \text{ g C m}^{-2} \text{ yr}^{-1}$  (Fig. 6),  
550 substantially larger than the MODIS derived value of around  $1,000 \text{ g C m}^{-2} \text{ yr}^{-1}$  from Yin et al.  
551 (2017) across central Africa, though it is important to note that satellite derived estimates of  
552 NPP can underestimate the impact of  $\text{CO}_2$  fertilization, namely its positive effect on  
553 photosynthesis (De Kauwe et al., 2016; Smith et al., 2019). Our stock of the present-day living  
554 biomass of 41.1 Pg C is relatively close to the total Congo vegetation biomass of 49.3 Pg C  
555 estimated by Verhegghen et al. (2012) based on the analysis of MERIS satellite data. Moreover,  
556 our simulated Congo Basin soil C stock of  $109 \pm 1.1 \text{ Pg C}$  is consistent with the approximately  
557 120-130 Pg C across Africa between the latitudes  $10^\circ\text{S}$  to  $10^\circ\text{N}$  in the review of Williams et  
558 al. (2007), between which the Congo represents roughly 70% of the land area. Therefore, their  
559 estimate of soil C stocks across the Congo only, would likely be marginally smaller than ours.  
560 It is also important to note that neither estimate of soil C stocks explicitly take into account the  
561 newly discovered peat store of 30 Pg C (Dargie et al., 2017) and therefore both are likely to  
562 represent conservative values. In addition, Williams et al. (2007) estimate the combined fluxes  
563 from conversion to agriculture and cultivation to be around  $100 \text{ Tg C yr}^{-1}$  in tropical Africa  
564 (largely synonymous with the Congo Basin), which is relatively close to our ~~present~~  
565 ~~day~~present-day estimate of harvesting + land-use change flux of  $170 \text{ Tg C yr}^{-1}$ .

566 Our results suggest that  $\text{CO}_2$  evasion from the water surfaces of the Congo is sustained by the  
567 transfer of dissolved  $\text{CO}_2$  and DOC with 226 Tg C and 73 Tg C, respectively, from wetland  
568 soils and vegetation to the aquatic system each year (1980-2010, Fig. 8). Moreover, we find  
569 that a disproportionate amount of this transfer occurs within the Cuvette Centrale wetland (Fig.  
570 1, Fig. 8) in the centre of the basin, in agreement with a recent study by Borges et al. (2019).  
571 In our study, this is due to the large areal proportion of inundated land, facilitating the exchange

572 between soils and aquatic systems. Borges et al. (2019) conducted measurements of DOC and  
573  $p\text{CO}_2$ , amongst other chemical variables, along the Congo mainstem and its tributaries from  
574 Kinshasa in the West of the basin (beside Brazzaville, Fig. 1) through the Cuvette Centrale to  
575 Kisangani in the East (close to station d in Fig. 1). They found that both DOC and  $p\text{CO}_2$   
576 approximately doubled from Kisangani downstream to Kinshasa (Table 3), and demonstrated  
577 that this variation is overwhelmingly driven by fluvial-wetland connectivity, highlighting the  
578 importance of the vast Cuvette Centrale wetland in the aquatic C budget of the Congo basin.

579 Our estimate of the integrated present-day aquatic  $\text{CO}_2$  evasion from the river surface of the  
580 Congo basin ( $32 \text{ Tg C yr}^{-1}$ ) is the same as that estimated by Raymond et al. (2013) (also  $32 \text{ Tg}$   
581  $\text{C yr}^{-1}$ ), downscaled over the same basin area, but smaller than the  $59.7 \text{ Tg C yr}^{-1}$  calculated by  
582 Lauerwald et al. (2015) and far smaller than that of Borges et al. (2015<sup>a</sup>),  $133\text{-}177 \text{ Tg C yr}^{-1}$  or  
583 Borges et al. (2019),  $251\pm 46 \text{ Tg C yr}^{-1}$ . The recent study of Borges et al. (2019) is based on by  
584 far and away the most extensive dataset of Congo basin  $p\text{CO}_2$  measurements to date and thus  
585 suggests that we substantially underestimate total riverine  $\text{CO}_2$  evasion. As previously  
586 discussed, we simulate the broad spatial and temporal variation in observed DOC and  $p\text{CO}_2$   
587 (2015<sup>a, b</sup>, Fig. 5, Table 3) relatively well. It is therefore somewhat surprising that our basin-  
588 wide estimate of riverine  $\text{CO}_2$  evasion is so different. Below we discuss some possible  
589 explanations for this discrepancy related to methodological differences and limitations.

590 One potential cause for the differences could be the river gas exchange velocity  $k$ . ~~However,~~  
591 ~~We~~ applied a mean riverine gas exchange velocity  $k_{600}$  of  $3.5 \text{ m d}^{-1}$  which is similar to the  $2.9$   
592  $\text{m d}^{-1}$  used by Borges et al. (2015<sup>a</sup>) but substantially smaller than the mean of approximately  $8$   
593  $\text{m d}^{-1}$  estimated across Strahler orders 1-10 in Borges et al. (2019) (taking the contributing  
594 water surface area of each Strahler order into account). ~~Moreover,~~ a sensitivity analysis was  
595 performed in Lauerwald et al. (2017) which showed that in the physical approach of  
596 ORCHILEAK,  $\text{CO}_2$  evasion is not very sensitive to the  $k$  value, unlike data-driven models.

597 Namely, Lauerwald et al (2017) showed that an increase or decrease of  $k_{600}$  for rivers and  
598 swamps (flooded forests) of 50% only led to 1% and -4% change in total CO<sub>2</sub> evasion,  
599 respectively. ~~Therefore, we can discount  $k$  as a major source of the discrepancy.~~ In  
600 ORCHILEAK,  $k$  does have an important impact on  $p\text{CO}_2$ ; i.e. a lower  $k$  value will increase  
601  $p\text{CO}_2$ , but this will also lead to a steeper water-air CO<sub>2</sub> gradient and so ultimately to  
602 approximately the same  $\text{FCO}_2$  over time. In other words, over the scales covered in this  
603 research (the large catchment area and water residence times of the Congo),  $\text{FCO}_2$  is mainly  
604 controlled by the allochthonous inputs of carbon to the river network, because by far the largest  
605 fraction of these C inputs is leaving the system via CO<sub>2</sub> emission to the atmosphere (as opposed  
606 to being laterally transferred downstream). Therefore, we do not consider  $k$  to be a major source  
607 of the discrepancy. Additionally, our  $k_{600}$  value of 0.65 m d<sup>-1</sup> for forested floodplains (based on  
608 Richey et al., 2002) compares well to recent a study which directly measured  $k_{600}$  on two  
609 different flooded forest sites in the Amazon basin, observing a range of 0.24 to 1.2 m d<sup>-1</sup>  
610 (MacIntyre et al., 2019).

611 Another potential reason for our smaller riverine CO<sub>2</sub> evasion could be river surface area. We  
612 simulate a mean present day (1980-2010) total river surface area of 25,900 km<sup>2</sup>, compared to  
613 the value of 23,670 km<sup>2</sup> used in Borges et al (2019, supplementary information) and so  
614 similarly we think that this can be discounted as a major source of discrepancy. However, it  
615 should be noted that both estimates are high compared to the recent estimate of 17,903 km<sup>2</sup>  
616 based on analysis of Landsat images (Allen & Pavelsky, 2018).

617 The difference in our simulated riverine CO<sub>2</sub> evasion compared to the empirically derived  
618 estimate of Borges et al. (2019), could be caused by the lack of representation of aquatic plants  
619 in the ORCHILEAK model. Borges et al. (2019) used the stable isotope composition of  $\delta^{13}\text{C}$ -  
620 DIC to determine the origin of dissolved CO<sub>2</sub> in the Congo River system and found that the  
621 values were consistent with a DIC input from the degradation of organic matter, in particular



622 from C<sub>4</sub> plants. Crucially, they further found that the  $\delta^{13}\text{C}$ -DIC values were unrelated to the  
623 contribution of *terra-firme* C<sub>4</sub> plants, rather that they were more consistent with the degradation  
624 of aquatic C<sub>4</sub> plants, namely macrophytes. ORCHILEAK does not represent aquatic plants, and  
625 the wider LSM ORCHIDEE does not have an aquatic macrophyte PFT either (though root  
626 respiration of floodplain plants for the PFTs represented, is accounted for as a C source). This  
627 could at the very least partly explain our conservative estimate of river CO<sub>2</sub> evasion, given that  
628 tropical macrophytes have relatively ~~elevated~~high NPPs. Rates as high as 3,500 g C m<sup>-2</sup> yr<sup>-1</sup>  
629 have been measured on floodplains in the Amazon (Silva et al., 2009). While this value is  
630 higher than the values simulated in the Cuvette Centrale by ORCHILEAK (Figure 8), they are  
631 of the same order of magnitude and so this alone cannot fully explain the discrepancy compared  
632 to the results of Borges et al. (2019). In the Amazon basin it has been shown that wetlands  
633 export approximately half of their gross primary production (GPP) to the river network  
634 compared to upland (*terra-firme*) ecosystems which only export a few percent (Abril et al.  
635 2013). More importantly, Abril et al. (2013) found that tropical aquatic macrophytes export  
636 80% of their GPP compared to just 36% for flooded forest. Therefore, the lack of a bespoke  
637 macrophyte PFT is indeed likely to be one reason for the discrepancy between our results and  
638 those of Borges, but largely due to their particularly high export efficiency to the river-  
639 floodplain network as opposed to differences in NPP. While being a significant limitation,  
640 creating and incorporating a macrophyte PFT would be a substantial undertaking given that the  
641 authors are unaware of any published dataset which has systematically mapped their  
642 distribution and abundance. It is important to note that while ORCHILEAK does not include  
643 the export of C from aquatic macrophytes it also neglects their NPP. Moreover, most aquatic  
644 macrophytes described in the literature have short (<1 year) life-cycles (Mitchel & Rogers,  
645 1985). As such, while this model limitation is likely one of the causes for our relatively low



646 estimate of riverine CO<sub>2</sub> evasion, it will only have a limited net effect on our estimate of the  
647 overall annual C balance (NBP, NEP) of the Congo basin.

648 Finally, another cause for the difference in riverine CO<sub>2</sub> evasion could be that the resolution of  
649 ORCHILEAK (0.5 degree river network and 1° for C fluxes) is not sufficient to fully capture  
650 the dynamics of the smallest streams of the Congo Basin which have been shown to have the  
651 highest DOC and CO<sub>2</sub> concentrations (Borges et al., 2019). Indeed, ORCHILEAK typically  
652 does not simulate the highest observed *p*CO<sub>2</sub> measurements of the smallest tributaries (i.e. >  
653 16,000 ppm). This is partly because for the fast reservoir (headwaters) in ORCHILEAK we  
654 assume full *p*CO<sub>2</sub> equilibrium with the atmosphere over one full day, which prevents very high  
655 *p*CO<sub>2</sub> values from building in the water column.

656 Despite these limitations, it is important to note that in our simulations, the evasion flux from  
657 rivers only contributes 15% of total aquatic CO<sub>2</sub> evasion, and including the flux from  
658 wetlands/floodplains, we produce a total of 235 Tg C yr<sup>-1</sup>. Moreover, the majority of this  
659 evasion occurs in the Cuvette Centrale (Fig. 8) which suggests that while ORCHILEAK fails to  
660 attribute a large portion of this flux to small rivers (owing to the coarse resolution of the river  
661 network) we nonetheless do capture the source of carbon. In other words, in ORCHILEAK the  
662 majority of this carbon evades directly from the floodplain and wetlands of the Cuvette  
663 Centrale as opposed to the small rivers.

664 Our simulated export of C to the coast of 15 (15.3) Tg C yr<sup>-1</sup> is virtually identical to the  
665 TOC+DIC export estimated by Borges et al. (2015<sup>a</sup>) of 15.5 Tg C yr<sup>-1</sup>, which is consistent with  
666 the fact that we simulate a similar spatial variation of DOC concentrations (Fig. 8 and Fig. 1  
667 for locations). It is also relatively similar to the 19 Tg C yr<sup>-1</sup> (DOC + DIC) estimated by  
668 Valentini et al. (2014) in their synthesis of the African carbon budget. Valentini et al. (2014)  
669 used the largely empirical based Global Nutrient Export from WaterSheds (NEWS) model

670 framework and they point out that Africa was underrepresented in the training data used to  
671 develop the regression relationships which underpin the model, and thus this could explain the  
672 small disagreement.

673 Of the total 15 Tg C yr<sup>-1</sup> exported to the coast, we simulate a 2.4 Tg C yr<sup>-1</sup> component of  
674 dissolved CO<sub>2</sub>, which is relatively similar to the empirically derived estimate of the total DIC  
675 export of 3.3 Tg C yr<sup>-1</sup> calculated in Wang et al. (2013). According to Wang et al., dissolved  
676 CO<sub>2</sub> accounts for the majority (1.9 Tg C yr<sup>-1</sup>) with the rest being the weathering derived flux  
677 of HCO<sub>3</sub><sup>-</sup>. Thus, the discrepancy between the two estimates is likely to be largely caused by  
678 our lack of accounting for the weathering derived flux (HCO<sub>3</sub><sup>-</sup>) which they estimate at 1.4 Tg  
679 C yr<sup>-1</sup>. In summary, despite this model limitation the results of Wang et al. (2013) suggest that  
680 we still capture the majority of the DIC flux.

681

## 682 **4.2 Trends in terrestrial and aquatic carbon fluxes**

683 There is relatively sparse observed data available on the long-term trends of terrestrial C fluxes  
684 in the Congo. Yin et al. (2017) used MODIS data to estimate NPP between 2001 and 2013  
685 across central Africa. They found that NPP increased on average by 10 g C m<sup>-2</sup> per year, while  
686 we simulate an average annual increase of 4 g C m<sup>-2</sup> yr<sup>-1</sup> over the same period across the Congo  
687 Basin. The two values are not directly comparable as they do not cover precisely the same  
688 geographic area but it is encouraging that our simulations exhibit a similar trend to remote  
689 sensing data. As previously noted, MODIS derived estimates of NPP do not fully include the  
690 effect of CO<sub>2</sub> fertilization (de Kauwe et al., 2016) whereas ORCHILEAK does. Thus, the  
691 MODIS NPP product may underestimate the increasing trend in NPP, which would bring our  
692 modeled trend further away from this dataset. On the other hand, forest degradation effects and

693 recent droughts have been associated with a decrease of greenness (Zhou et al., 2014) and  
694 above ground biomass loss (Qie et al., 2019) in tropical forests.

695 Up to a point, our results also concur with estimates based on the upscaling of biomass  
696 observations (Lewis et al., 2009; Hubau et al., 2019). Lewis et al. (2009) up-scaled forest plot  
697 measurements to calculate that intact tropical African forests represented a net uptake of  
698 approximately 300 Tg C yr<sup>-1</sup> between 1968 and 2007 and this is consistent with our NEP  
699 estimate of 275 Tg C yr<sup>-1</sup> over the same period. However, more recently an analysis based on  
700 an extension of the same dataset found that the above ground C sink in tropical Africa was  
701 relatively stable from 1985 to 2015 (Hubau et al., 2020).

702 A major source of the uncertainty associated with future projections of NPP and NEP comes  
703 from our limited understanding and representation of the CO<sub>2</sub> fertilization effect. Recent  
704 analysis of data from some of the longest-running Free-Air CO<sub>2</sub> Enrichment (FACE) sites,  
705 consisting of early-successional temperate ecosystems, found a 29.1 ± 11.7% stimulation of  
706 biomass over a decade (Walker et al., 2019). A meta-analysis (Liu et al., 2019) of seven  
707 temperate FACE experiments combined with process-based modelling also found substantial  
708 sensitivity (0.64 ± 0.28 PgC yr<sup>-1</sup> per hundred ppm) of biomass accumulation to atmospheric  
709 CO<sub>2</sub> increase, and the same study showed that ORCHIDEE model simulations were largely  
710 consistent with the experiments. However, other FACE experiments on mature temperate  
711 forests (Körner et al., 2005), as well as eucalyptus forests bring into question whether the  
712 fertilization effects observed in temperate FACE experiments can be extrapolated to other  
713 ecosystems. For example, the Swiss FACE study, a deciduous mature forest, found no  
714 significant biomass increase with enhanced CO<sub>2</sub> (Körner et al., 2005), while a FACE  
715 experiment on a mature eucalyptus forest in Australia found that while CO<sub>2</sub> stimulated an  
716 increase in C uptake through GPP, this did not carry to the ecosystem level, largely as a result  
717 of a concurrent increase in soil respiration (Jiang et al., 2020). Unfortunately, no results are yet

718 available from any tropical FACE experiments, though the Amazon FACE experiment is  
719 underway and the eventual results will be crucial in developing our understanding of the CO<sub>2</sub>  
720 fertilization effect beyond the temperate zone.

721 With these limitations in our understanding of tropical forest ecosystems in mind, over the  
722 entire simulation period (1861-2099) we estimate that aquatic CO<sub>2</sub> evasion will increase by

723 79% and the export of C to the coast by 67%. While, there are no long-term observations of  
724 aquatic CO<sub>2</sub> evasion in the Congo, a recent paper examined trends in observed DOC fluxes in  
725 the Congo at Brazzaville/Kinshasa over the last 30 years (Moukandi N'kaya et al. 2020). They  
726 found a 45% increase in the annual flux of DOC from 11.1 Tg C yr<sup>-1</sup> (mean from 1987-1993)  
727 to 16.1 Tg C yr<sup>-1</sup> (mean from 2006-2017). Comparing the same two periods, we find a smaller  
728 increase of 15% from 12.3 Tg C yr<sup>-1</sup> to 14.2 Tg C yr<sup>-1</sup>. While our increase is substantially  
729 smaller, these observations are still over relatively short time scales and thus interannual  
730 variations could have considerable influence over the means of the two periods. Irrespectively  
731 it is encouraging that observations concur with the overall simulated increasing trend. Perhaps  
732 most interesting is that Moukandi N'kaya et al. (2020) attribute this increase to hydrological  
733 changes and specifically an increase in flood events in the central basin (including the Cuvette  
734 Centrale). Over this period, we too attribute the increase in carbon fluxes to the coast in part to  
735 climate change (Fig. 11 d) and over the full simulation period, the largest increase in DOC and  
736 CO<sub>2</sub> leaching into the aquatic system occurs within the Cuvette Centrale (Fig. A1).

737 Comparing our results to models of other basins, our simulated increases in outgassing (79%)  
738 and the export of C to the coast (67%). This increase ~~are~~ is considerably ~~higher~~ ~~greater~~ than the

739 23% and 27% ~~rise~~ ~~in outgassing and export~~ predicted for the Amazon basin (Lauerwald et al.,  
740 2020), over the same period and under the same scenario. This is largely due to the fact climate  
741 change is predicted to have a substantial negative impact on the aquatic C fluxes in the Amazon,  
742 something that we do not find for the Congo where rainfall is projected to substantially increase

743 over the 21<sup>st</sup> century (RCP 6.0). In the Amazon, Lauerwald et al. (2020) show that while there  
744 are decadal fluctuations in precipitation and discharge, total values across the basin remain  
745 unchanged in 2099 compared to 1861. However, changes in the spatial distribution of  
746 precipitation mean that the total water surface area actually decreases in the Amazon. Indeed,  
747 while we find an increase in the ratio of C exports to the LOAC/NPP from 3 to 5%, Lauerwald  
748 et al. (2020) find a comparative decrease.

749 Our simulated increase in DOC export to the coast up to the present day is smaller than findings  
750 recently published for the Mississippi River using the Dynamic Land Ecosystem Model  
751 (DLEM, Ren et al., 2016). In addition, the Mississippi study identified LUC including land  
752 management practices (e.g. irrigation and fertilization), followed by change in atmospheric  
753 CO<sub>2</sub>, as the biggest factors in the 40% increase in DOC export to the Gulf of Mexico (Ren et  
754 al., 2016). Another recent study (Tian et al., 2015), found an increase in DIC export from  
755 eastern North America to the Atlantic Ocean from 1901-2008 but no significant trend in DOC.  
756 They demonstrated that climate change and increasing atmospheric CO<sub>2</sub> had a significant  
757 positive effect on long-term C export while land-use change had a substantial negative impact.

### 758 **4.3 Limitations and further model developments**

759 It is important to note that we can have greater confidence in the historic trend (until present-  
760 day), as the future changes are more reliant on the skill of Earth System model predictions and  
761 of course on the accuracy of the RCP 6.0 scenario. As discussed above, our understanding and  
762 representation of CO<sub>2</sub> fertilization, especially in the tropics, is a major limitation. Moreover,  
763 the majority of land surface models, ORCHILEAK included in its current iteration, do not  
764 represent the effect of nutrient limitation on plant growth meaning that estimates of land C  
765 uptake may be too large (Goll et al., 2017). There are also considerable uncertainties associated  
766 with future climate projections in the Congo basin (Haensler et al., 2013). Nutrient limitation

767 on growth and a better representation of effect of enhanced CO<sub>2</sub>, particularly with regards to  
768 soil respiration (Jiang et al., 2020) and tree mortality (Hubau et al., 2020), are two crucial  
769 aspects which need to be further developed.

770 Additionally, we do not account for methane fluxes from Congo wetlands, estimated at 1.6 to  
771 3.2 Tg (CH<sub>4</sub>) per year (Tathy et al., 1992), and instead assume that all C is evaded in the form  
772 of CO<sub>2</sub>. Another limitation is the lack of accounting for bespoke peatland dynamics in the  
773 ORCHILEAK model. ORCHILEAK is able to represent the general reduction in C  
774 decomposition in water-logged soils and indeed Hastie et al. (2019) demonstrated that  
775 increasing the maximum floodplain extent in the Amazon Basin led to an increase in NEP  
776 despite fueling aquatic CO<sub>2</sub> evasion because of the effect of reducing soil heterotrophic  
777 respiration. Furthermore, ORCHILEAK uses a “poor soils” mask forcing file (Fig. 2 j) based  
778 on the Harmonized World Soil Database (FAO/IIASA/ISRIC/ISS-CAS/JRC, 2009), which  
779 prescribes reduced decomposition rates in low nutrient and pH soils (e.g. Podzols and  
780 Arenosols). The effect of the “poor soils” forcing can clearly be seen in the spatial distribution  
781 of the soil C stock in Fig. A3, where the highest C storage coincides with the highest proportion  
782 of poor soils. Interestingly, this does not include the Cuvette Centrale wetlands (Fig. 1), an area  
783 which was recently identified as containing the world’s largest intact tropical peatland and a  
784 stock of around 30 Pg C (Dargie et al., 2017). One potential improvement that could be made  
785 to ORCHILEAK would be the development of a new tailored “poor soils” forcing file for the  
786 Congo Basin which explicitly includes Histosols, perhaps informed by the Soil Grids database  
787 (Hengl et al., 2014), to better represent the Cuvette Centrale. This could in turn, be validated  
788 and/or calibrated against the observations of Dargie et al. (2017). A more long-term aim could  
789 be the integration/ coupling of the ORCHIDEE-PEAT module with ORCHILEAK.  
790 ORCHIDEE-PEAT (Qiu et al., 2019) represents peat as an independent sub-grid hydrological  
791 soil unit in which peatland soils are characterized by peat-specific hydrological properties and

792 multi-layered transport of C and water. Thus far, it has only been applied to northern peatlands,  
793 and calibrating it to tropical peatlands, along with integrating it within ORCHILEAK would  
794 require considerable further model development, but would certainly be a valuable longer-term  
795 aspiration. This could also be applied across the tropical region and would allow us to  
796 comprehensively explore the implications of climate change and land-use change for tropical  
797 peatlands. In addition, ORCHILEAK does not simulate the erosion and subsequent burial of  
798 POC within river and floodplain sediments. Although it does not represent the lateral transfer  
799 of POC, it does incorporate the decomposition of inundated litter as an important source of  
800 DOC and dissolved CO<sub>2</sub> to the aquatic system; i.e. it is assumed that POC from submerged  
801 litter decomposes locally in ORCHILEAK. Moreover, previous studies have found that DOC  
802 as opposed to POC (Spencer et al., 2016; Bouillon et al., 2012) overwhelmingly dominates the  
803 total load of C in the Congo.

804 The representation of the rapid C loop of aquatic macrophytes should also be made a priority  
805 in terms of improving models such as ORCHILEAK, particularly in the tropics. As previously  
806 discussed, ORCHILEAK also fails to account for the weathering derived flux (HCO<sub>3</sub><sup>-</sup>). Finally,  
807 the issue of shifting cultivation demands further attention; at least for the present day a shifting  
808 cultivation forcing file could be developed based on remote sensing data (Tyukavina et al.,  
809 2018). For additional discussion of the limitations of ORCHILEAK, please also see Lauerwald  
810 et al. (2017) and Hastie et al. (2019).

## 811 **5. Conclusions**

812 For the present day, we show that aquatic C fluxes, and in particular CO<sub>2</sub> evasion, are important  
813 components of the Congo Basin C balance, larger than for example the combined fluxes from  
814 LUC and harvesting, with around 4% of terrestrial NPP being exported to the aquatic system  
815 each year. Our simulations show that these fluxes may have undergone considerable

816 perturbation since 1861 to the present day, and that under RCP 6.0 this perturbation could  
817 continue; over the entire simulation period (1861-2099), we estimate that aquatic CO<sub>2</sub> evasion  
818 will increase by 79% and the export of C to the coast by 67%. We further find that the ratio of  
819 C exports to the LOAC/NPP could increase from 3 to 5%, driven by both rising atmospheric  
820 CO<sub>2</sub> concentrations and climate change. This calls for long-term monitoring of C levels and  
821 fluxes in the rivers of the Congo basin, and further investigation of the potential impacts of  
822 such change. Our results also highlight the limitations of the current generation of land surface  
823 models and call for investment into further model development.

824

825 *Code availability.* A description of the general ORCHIDEE code can be found here:  
826 [http://forge.ipsl.jussieu.fr/orchidee/browser#tags/ORCHIDEE\\_1\\_9\\_6/ORCHIDEE](http://forge.ipsl.jussieu.fr/orchidee/browser#tags/ORCHIDEE_1_9_6/ORCHIDEE).

827 The main part of the ORCHIDEE code was written by Krinner et al. (2005). See d'Orgeval et  
828 al. (2008) for a general description of the river routing scheme. For the updated soil C module  
829 please see Camino Serrano (2015). For the source code of ORCHILEAK see Lauerwald et al.  
830 (2017)- <https://doi.org/10.5194/gmd-10-3821-2017-supplement>

831 For details on how to install ORCHIDEE and its various branches, please see the user guide:  
832 <http://forge.ipsl.jussieu.fr/orchidee/wiki/Documentation/UserGuide>

833 *Author contribution.* AH, RL, PR and PC all contributed to the conceptualization of the study.  
834 RL developed the model code, AH developed the novel forcing files for Congo, and AH  
835 performed the simulations. FP provided the GIEMS dataset for model validation. AH prepared  
836 the manuscript with contributions from all co-authors. RL and PR provided supervision and  
837 guidance to AH throughout the research. PR acquired the primary financial support that  
838 supported this research.

839 *Competing interests.* The authors declare that they have no conflict of interest.



840 *Financial support.* Financial support was received from the European Union's Horizon 2020  
841 research and innovation programme under the Marie Skłodowska- Curie grant agreement No.  
842 643052 (C-CASCADES project). AH acknowledges funding from the UK *Natural*  
843 *Environment Research Council (NE/R000751/1)*. PR acknowledges funding from the European  
844 Union's Horizon 2020 research and innovation programme under Grant Agreement 776810  
845 (project VERIFY). RL acknowledges funding from the ANR ISIPEDIA ERA4CS project and  
846 from the French state aid managed by the ANR under the  
847 'Investissements d'avenir' programme with the reference ANR-16-CONV-0003.

848

## 849 **References**

- 850 Abril, G., Martinez, J.-M., Artigas, L. F., Moreira-Turcq, P., Benedetti, M. F., Vidal, L., ...  
851 Roland, F. (2013). Amazon River carbon dioxide outgassing fuelled by wetlands. *Nature*,  
852 505, 395. Retrieved from <http://dx.doi.org/10.1038/nature12797>
- 853 ~~Battin, T. J., Luysaert, S., Kaplan, L. A., Aufdenkampe, A. K., Richter, A., & Tranvik, L. J.~~  
854 ~~(2009). The boundless carbon cycle. *Nature Geoscience*, 2, 598. Retrieved from~~  
855 ~~<https://doi.org/10.1038/ngeo618>~~
- 856 Allen, G. H., & Pavelsky, T. M. (2018). Global extent of rivers and streams. *Science*,  
857 361(6402), 585–588. <https://doi.org/10.1126/science.aat0636>
- 858 Becker, M.; Papa, F.; Frappart, F.; Alsdorf, D.; Calmant, S.; Da Silva, J.S.; Prigent, C.;  
859 Seyler, F. Satellite-based estimates of surface water dynamics in the Congo River Basin. *Int.*  
860 *J. Appl. Earth Obs. Geoinf.* 2018, 196–209
- 861 Borges, A. V, Darchambeau, F., Teodoru, C. R., Marwick, T. R., Tamooh, F., Geeraert, N.,  
862 ... Bouillon, S. (2015)<sup>a</sup>. Globally significant greenhouse-gas emissions from African inland  
863 waters. *Nature Geoscience*, 8, 637. Retrieved from <https://doi.org/10.1038/ngeo2486>
- 864 Borges, A. V, Abril, G., Darchambeau, F., Teodoru, C. R., Deborde, J., Vidal, L. O., ...  
865 Bouillon, S. (2015)<sup>b</sup>. Divergent biophysical controls of aquatic CO<sub>2</sub> and CH<sub>4</sub> in the World's  
866 two largest rivers. *Scientific Reports*, 5, 15614. <https://doi.org/10.1038/srep15614>
- 867 Borges, A. V., Darchambeau, F., Lambert, T., Morana, C., Allen, G. H., Tambwe, E.,  
868 Toengaho Sembaito, A., Mambo, T., Nlandu Wabakhangazi, J., Descy, J.-P., Teodoru, C. R.,  
869 and Bouillon, S (2019).: Variations in dissolved greenhouse gases (CO<sub>2</sub>, CH<sub>4</sub>, N<sub>2</sub>O) in the  
870 Congo River network overwhelmingly driven by fluvial-wetland connectivity,  
871 *Biogeosciences*, 16, 3801–3834, <https://doi.org/10.5194/bg-16-3801-2019>.

872 Bouillon, S., Yambélé, A., Spencer, R. G. M., Gillikin, D. P., Hernes, P. J., Six, J., Merckx,  
873 R., and Borges, A. V.: Organic matter sources, fluxes and greenhouse gas exchange in the  
874 Oubangui River (Congo River basin), *Biogeosciences*, 9, 2045–2062,  
875 <https://doi.org/10.5194/bg-9-2045-2012>, 2012.

876 Bouillon, S., Yambélé, A., Gillikin, D. P., Teodoru, C., Darchambeau, F., Lambert, T., &  
877 Borges, A. V. (2014). Contrasting biogeochemical characteristics of the Oubangui River and  
878 tributaries (Congo River basin). *Scientific Reports*, 4, 5402. Retrieved from  
879 <https://doi.org/10.1038/srep05402>

880 Bowring, S. P. K., Lauerwald, R., Guenet, B., Zhu, D., Guimberteau, M., Tootchi, A.,  
881 Ducharne, A., and Ciais, P (2019)<sup>a</sup>: ORCHIDEE MICT-LEAK (r5459), a global model for  
882 the production, transport, and transformation of dissolved organic carbon from Arctic  
883 permafrost regions – Part 1: Rationale, model description, and simulation protocol, *Geosci.*  
884 *Model Dev.*, 12, 3503–3521, <https://doi.org/10.5194/gmd-12-3503-2019>, 2019.

885 Bowring, S. P. K., Lauerwald, R., Guenet, B., Zhu, D., Guimberteau, M., Regnier, P.,  
886 Tootchi, A., Ducharne, A., and Ciais, P (2019)<sup>b</sup>: ORCHIDEE MICT-LEAK (r5459), a global  
887 model for the production, transport and transformation of dissolved organic carbon from  
888 Arctic permafrost regions, Part 2: Model evaluation over the Lena River basin, *Geosci.*  
889 *Model Dev. Discuss.*, <https://doi.org/10.5194/gmd-2018-322>, in review, 2019.

890 Camino-Serrano, M., Guenet, B., Luyssaert, S., Ciais, P., Bastrikov, V., De Vos, B., Gielen,  
891 B., Gleixner, G., Jornet-Puig, A., Kaiser, K., Kothawala, D., Lauerwald, R., Peñuelas, J.,  
892 Schrumpp, M., Vicca, S., Vuichard, N., Walmsley, D., and Janssens, I. A.: ORCHIDEE-  
893 SOM: modeling soil organic carbon (SOC) and dissolved organic carbon (DOC) dynamics  
894 along vertical soil profiles in Europe, *Geosci. Model Dev.*, 11, 937–957,  
895 <https://doi.org/10.5194/gmd-11-937-2018>, 2018

896 CBFP (Congo Basin Forest Partnership) (2009). The forests of the Congo Basin — State of  
897 the Forest 2008, Publications Office of the European  
898 Union, Luxembourg (2009), 10.2788/32259

899 Ciais, P., Piao, S.-L., Cadule, P., Friedlingstein, P., & Chédin, A. (2009). Variability and  
900 recent trends in the African terrestrial carbon balance. *Biogeosciences*, 6(9), 1935–1948.  
901 <https://doi.org/10.5194/bg-6-1935-2009>

902 Ciais, P., Yao, Y., Gasser, T., Baccini, A., Wang, Y., Lauerwald, R., ... Zhu, D. (2020).  
903 Empirical estimates of regional carbon budgets imply reduced global soil heterotrophic  
904 respiration. *National Science Review*. <https://doi.org/10.1093/nsr/nwaa145>

905 Cochonneau, G., Sondag, F., Guyot, J.-L., Geraldo, B., Filizola, N., Fraizy, P., Laraque, A.,  
906 Magat, P., Martinez, J.-M., Noriega, L., Oliveira, E., Ordonez, J., Pombosa, R., Seyler, F.,  
907 Sidgwick, J., and Vauchel, P.: The environmental observation and research project, ORE  
908 HYBAM, and the rivers of the Amazon basin, in: Climate Variability and Change –  
909 Hydrological Impacts, IAHS Publ. 308, edited by: Demuth, S., Gustard, A., Planos, E.,  
910 Scatena, F., and Servat, E., IAHS Press, UK, 44–50, 2006

911 Coynel, A., P. Seyler, H. Etcheber, M. Meybeck, and D. Orange (2005), Spatial and seasonal  
912 dynamics of total suspended sediment and organic carbon species in the Congo River, *Global*  
913 *Biogeochem. Cycles*, 19, GB4019, doi:[10.1029/2004GB002335](https://doi.org/10.1029/2004GB002335).

914 Creese, A., Washington, R., & Jones, R. (2019). Climate change in the Congo Basin:  
915 processes related to wetting in the December–February dry season. *Climate Dynamics*, 53(5),  
916 3583–3602. <https://doi.org/10.1007/s00382-019-04728-x>

917 Dargie, G. C., Lewis, S. L., Lawson, I. T., Mitchard, E. T. A., Page, S. E., Bocko, Y. E., &  
918 Ifo, S. A. (2017). Age, extent and carbon storage of the central Congo Basin peatland  
919 complex. *Nature*, 542, 86. Retrieved from <https://doi.org/10.1038/nature21048>

920 De Kauwe, M. G., Keenan, T. F., Medlyn, B. E., Prentice, I. C. and Terrer. C. (2016) Satellite  
921 based estimates underestimate the effect of CO<sub>2</sub> fertilisation on net primary  
922 productivity. *Nature Climate Change*, 6, 892-893

923 d'Orgeval, T., Polcher, J., & de Rosnay, P. (2008). Sensitivity of the West African  
924 hydrological cycle in ORCHIDEE to infiltration processes. *Hydrology and Earth System  
925 Sciences*, 12, 1387– 1401. <https://doi.org/10.5194/hess-12-1387-2008>

926 Drake, T. W., Raymond, P. A., & Spencer, R. G. M. (2018). Terrestrial carbon inputs to  
927 inland waters: A current synthesis of estimates and uncertainty. *Limnology and  
928 Oceanography Letters*, 3(3), 132–142. <http://doi.org/10.1002/lol2.10055>

929 Fan, L., Wigneron, J.-P., Ciais, P., Chave, J., Brandt, M., Fensholt, R., ... Peñuelas, J. (2019).  
930 Satellite-observed pantropical carbon dynamics. *Nature Plants*, 5(9), 944–951.  
931 <https://doi.org/10.1038/s41477-019-0478-9>

932 FAO/IIASA/ISRIC/ISS-CAS/JRC: Harmonized World Soil Database (version 1.1), FAO,  
933 Rome, 2009.

934 Fisher JB, Sikka M, Sitch S, Ciais P, Poulter B, Galbraith D, Lee J-E, Huntingford C, Viogy  
935 N, Zeng N, Ahlstrom A, Lomas MR, Levy PE, Frankenberg C, Saatchi S, Malhi Y. 2013  
936 African tropical rainforest net carbon dioxide fluxes in the twentieth century. *Phil Trans R  
937 Soc B* 368: 20120376.<http://dx.doi.org/10.1098/rstb.2012.0376>

938 Frieler, K., Lange, S., Piontek, F., Reyer, C. P. O., Schewe, J., Warszawski, L., ... Yamagata,  
939 Y. (2017). Assessing the impacts of 1.5 °C global warming – simulation protocol of the Inter-  
940 Sectoral Impact Model Intercomparison Project (ISIMIP2b). *Geosci. Model Dev.*, 10(12),  
941 4321–4345. <https://doi.org/10.5194/gmd-10-4321-2017>

942 Goll, D. S., Vuichard, N., Maignan, F., Jornet-Puig, A., Sardans, J., Violette, A., Peng, S.,  
943 Sun, Y., Kvakic, M., Guimberteau, M., Guenet, B., Zaehle, S., Penuelas, J., Janssens, I., and  
944 Ciais, P.: A representation of the phosphorus cycle for ORCHIDEE (revision 4520), *Geosci.  
945 Model Dev.*, 10, 3745-3770, <https://doi.org/10.5194/gmd-10-3745-2017>, 2017.

946 Guimberteau, M., Drapeau, G., Ronchail, J., Sultan, B., Polcher, J., Martinez, J.-M., Prigent,  
947 C., Guyot, J.-L., Cochonneau, G., Espinoza, J. C., Filizola, N., Fraizy, P., Lavado, W., De  
948 Oliveira, E., Pombosa, R., Noriega, L., and Vauchel, P.: Discharge simulation in the sub-  
949 basins of the Amazon using ORCHIDEE forced by new datasets, *Hydrol. Earth Syst. Sci.*, 16,  
950 911–935, <https://doi.org/10.5194/hess-16-911-2012>, 2012.

951 Gumbrecht, T., Roman-Cuesta, R. M., Verchot, L., Herold, M., Wittmann, F., Householder,  
952 E., Murdiyarso, D. (2017). An expert system model for mapping tropical wetlands and  
953 peatlands reveals South America as the largest contributor. *Global Change Biology*, 23(9),  
954 3581–3599. <https://doi.org/10.1111/gcb.13689>

955 Haensler, A., Saeed, F. and Jacob, D. (2013): Assessment of projected climate change signals  
956 over central Africa based on a multitude of global and regional climate projections. In:  
957 Climate Change Scenarios for the Congo Basin. [Haensler A., Jacob D., Kabat P., Ludwig F.  
958 (eds.)]. Climate Service Centre Report No. 11, Hamburg, Germany, ISSN: 2192-4058

959 Hastie, A., Lauerwald, R., Ciais, P., Regnier, P (2019). Aquatic carbon fluxes dampen the  
960 overall variation of net ecosystem productivity in the Amazon basin: An analysis of the  
961 interannual variability in the boundless carbon cycle. *Global Change*  
962 *Biology*,; 25: 2094– 2111. <https://doi.org/10.1111/gcb.14620>

963 Hartmann, J., R. Lauerwald, and N. Moosdorf (2014), A brief overview of the GLObal RIver  
964 CHemistry Database, GLORICH, Procedia Earth Planet. Sci., **10**, 23–27.

965 Heinimann A, Mertz O, Frohking S, Egelund Christensen A, Hurni K, Sedano F, et al. (2017)  
966 A global view of shifting cultivation: Recent, current, and future extent. PLoS ONE 12(9):  
967 e0184479. <https://doi.org/10.1371/journal.pone.0184479>

968 Hengl, T., de Jesus, J. M., MacMillan, R. A., Batjes, N. H., Heuvelink, G. B. M., Ribeiro, E.,  
969 ... Ruiperez Gonzalez, M. (2014). SoilGrids1km-global soil information based on automated  
970 mapping. PLoS One, 9, e105992. <https://doi.org/10.1371/journal.pone.0105992>

971 Hubau, W.; Lewis, S.L.; Phillips, O.L.; Affum-Baffoe, K.; Beeckman, H.; Cuní-Sanchez, A.;  
972 Daniels, A.K.; Ewango, C.E.N.; Fauset, S.; Mukinzi, J.M.; et al. Asynchronous carbon sink  
973 saturation in African and Amazonian tropical forests. *Nature* 2020, 579, 80–87.

974 Hurtt, G. C., Chini, L. P., Frohking, S., Betts, R. A., Feddema, J., Fischer, G., ... Wang, Y. P.  
975 (2011). Harmonization of land-use scenarios for the period 1500--2100: 600 years of global  
976 gridded annual land-use transitions, wood harvest, and resulting secondary lands. *Climatic*  
977 *Change*, 109(1), 117. <https://doi.org/10.1007/s10584-011-0153-2>

978 Jiang, M., Medlyn, B.E., Drake, J.E. *et al.* The fate of carbon in a mature forest under carbon  
979 dioxide enrichment. *Nature* **580**, 227–231 (2020). <https://doi.org/10.1038/s41586-020-2128-9>

980 Kim, H. (2017). *Global Soil Wetness Project Phase 3 Atmospheric Boundary Conditions*  
981 *(Experiment 1)* [Data set]. Data Integration and Analysis System (DIAS).  
982 <https://doi.org/10.20783/DIAS.501>

983 Korner C, Asshoff R, Bignucolo O (2005) Carbon flux and growth in mature deciduous forest  
984 trees exposed to elevated CO2. *Science*, 309, 1360–1362.

985 Lange., S (2017). "ISIMIP2b Bias-Correction Code," *Zenodo*, doi: [10.5281/zenodo.1069050](https://doi.org/10.5281/zenodo.1069050)

986 Laudon, H., and I. Buffam (2008), Impact of changing DOC concentrations on the potential  
987 distribution of acid sensitive biota in a boreal stream network, *Hydrol. Earth Syst.*  
988 *Sci.*, **12**(2), 425–435.

989 Lauerwald, R., Laruelle, G. G., Hartmann, J., Ciais, P., & Regnier, P. A. G. (2015). Spatial  
990 patterns in CO2 evasion from the global river network. *Global Biogeochemical Cycles*, 29(5),  
991 534–554. <https://doi.org/10.1002/2014GB004941>

992 Lauerwald, R., Regnier, P., Camino-Serrano, M., Guenet, B., Guimberteau, M., Ducharne,  
993 A., ... Ciais, P. (2017). ORCHILEAK (revision 3875): a new model branch to simulate

994 carbon transfers along the terrestrial--aquatic continuum of the Amazon basin. *Geoscientific*  
995 *Model Development*, 10(10), 3821–3859. <https://doi.org/10.5194/gmd-10-3In821-2017>

996 Lauerwald, R., Regnier, P., Guenet, B., Friedlingstein, P; Ciais, P (2020): How simulations of  
997 the land carbon sink are biased by ignoring fluvial carbon transfers – A case study for the  
998 Amazon basin. *One Earth*, 10.1016/j.oneear.2020.07.009.

999 Lee, H., Beighley, R. E., Alsdorf, D., Jung, H. C., Shum, C. K., Duan, J., ... Andreadis, K.  
1000 (2011). Characterization of terrestrial water dynamics in the Congo Basin using GRACE and  
1001 satellite radar altimetry. *Remote Sensing of Environment*, 115(12), 3530–3538.  
1002 <https://doi.org/https://doi.org/10.1016/j.rse.2011.08.015>

1003 Lehner, B., & Döll, P. (2004). Development and validation of a global database of lakes,  
1004 reservoirs and wetlands. *Journal of Hydrology*, 296(1–4), 1–22.  
1005 <https://doi.org/https://doi.org/10.1016/j.jhydrol.2004.03.028>

1006 Lewis, S. L., Lopez-Gonzalez, G., Sonké, B., Affum-Baffoe, K., Baker, T. R., Ojo, L. O., ...  
1007 Wöll, H. (2009). Increasing carbon storage in intact African tropical forests. *Nature*, 457,  
1008 1003. Retrieved from <https://doi.org/10.1038/nature07771>

1009 Liu, Y., Piao, S., Gasser, T., Ciais, P., Yang, H., Wang, H., ... Wang, T. (2019). Field-  
1010 experiment constraints on the enhancement of the terrestrial carbon sink by CO2 fertilization.  
1011 *Nature Geoscience*, 12(10), 809–814. <https://doi.org/10.1038/s41561-019-0436-1>

1012 [MacIntyre, S., Amaral, J. H. F., Barbosa, P. M., Cortés, A., Forsberg, B. R., & Melack, J.](#)  
1013 [M. \(2019\). Turbulence and gas transfer velocities in sheltered flooded forests of the Amazon](#)  
1014 [Basin. \*Geophysical Research\*](#)  
1015 [Letters, 46, 9628– 9636. <https://doi.org/10.1029/2019GL083948>](#)

1016 Masui, T., Matsumoto, K., Hijioka, Y., Kinoshita, T., Nozawa, T., Ishiwatari, S., Kato, E.,  
1017 Shukla, P.R., Yamagata, Y., Kainuma, M., 2011. A emission pathway to stabilize at 6 W/m2  
1018 of radiative forcing, *Climatic Change*, doi:10.1007/s10584-011-0150-5. Morgan, M.G.,  
1019 Adams, P., Keith, D.W., 2006. Elicitation of expert judgments of aerosol forcing. *Climatic*  
1020 *Change* 75, 195–214

1021 Melack, J.M., Hess, L.L., Gastil, M., Forsberg, B.R., Hamilton, S.K., Lima, I.B. and Novo,  
1022 E.M. (2004), Regionalization of methane emissions in the Amazon Basin with microwave  
1023 remote sensing. *Global Change Biology*, 10: 530-544. doi:[10.1111/j.1365-2486.2004.00763.x](https://doi.org/10.1111/j.1365-2486.2004.00763.x)

1024 Mitchell D.S., Rogers K.H. (1985) Seasonality/aseasonality of aquatic macrophytes in  
1025 Southern Hemisphere inland water. In: Davies B.R., Walmsley R.D. (eds) *Perspectives in*  
1026 *Southern Hemisphere Limnology*. Developments in Hydrobiology, vol 28. Springer,  
1027 Dordrecht

1028 [Moukandi N’kaya et al. \(2020\) Temporal Variability of Sediments, Dissolved Solids and](#)  
1029 [Dissolved Organic Matter Fluxes in the Congo River at Brazzaville/Kinshasa, \*Geosciences\*](#)  
1030 [2020, 10, 341; doi:10.3390/geosciences10090341](#)

1031 Nash, J. E., and J. V. Sutcliffe. 1970. River flow forecasting through conceptual models: Part  
1032 1. A discussion of principles. *J. Hydrology* 10(3): 282-290



1033 O'Loughlin, F., M. A. Trigg, G. J.-P. Schumann, and P. D. Bates (2013), Hydraulic  
1034 characterization of the middle reach of the Congo River, *Water Resour. Res.*, 49, 5059–5070,  
1035 doi:[10.1002/wrcr.20398](https://doi.org/10.1002/wrcr.20398).

1036 Pan, S., Dangal, S. R. S., Tao, B., Yang, J., & Tian, H. (2015). Recent patterns of terrestrial  
1037 net primary production in Africa influenced by multiple environmental changes. *Ecosystem*  
1038 *Health and Sustainability*, 1(5), 1–15. <https://doi.org/10.1890/EHS14-0027.1>

1039 Papa, F., Prigent, C., Aires, F., Jimenez, C., Rossow, W. B., and Matthews,  
1040 E. (2010), Interannual variability of surface water extent at the global scale, 1993–2004, *J.*  
1041 *Geophys. Res.*, 115, D12111, doi:[10.1029/2009JD012674](https://doi.org/10.1029/2009JD012674).

1042 Potapov, P. V., Turubanova, S. A., Hansen, M. C., Adusei, B., Broich, M., Altstatt, A., ...  
1043 Justice, C. O. (2012). Quantifying forest cover loss in Democratic Republic of the Congo,  
1044 2000–2010, with Landsat ETM+ data. *Remote Sensing of Environment*, 122, 106–116.  
1045 <https://doi.org/https://doi.org/10.1016/j.rse.2011.08.027>

1046 Potter, C., Klooster, S., & Genovese, V. (2012). Net primary production of terrestrial  
1047 ecosystems from 2000 to 2009. *Climatic Change*, 115(2), 365–378.  
1048 <https://doi.org/10.1007/s10584-012-0460-2>

1049 Prigent, C., Papa, F., Aires, F., Rossow, W. B., and Matthews, E.: Global inundation  
1050 dynamics inferred from multiple satellite observations, 1993–2000, *J. Geophys. Res.*, 112,  
1051 D12107, <https://doi.org/10.1029/2006jd007847>, 2007.

1052 Qie, L., Telford, E. M., Massam, M. R., Tangki, H., Nilus, R., Hector, A., & Ewers, R. M.  
1053 (2019). Drought cuts back regeneration in logged tropical forests. *Environmental Research*  
1054 *Letters*, 14(4), 45012. <https://doi.org/10.1088/1748-9326/ab0783>

1055 Qiu, C., Zhu, D., Ciais, P., Guenet, B., Peng, S., Krinner, G., Tootchi, A., Ducharne, A., and  
1056 Hastie, A.: Modelling northern peatland area and carbon dynamics since the Holocene with  
1057 the ORCHIDEE-PEAT land surface model (SVN r5488), *Geosci. Model Dev.*, 12, 2961–  
1058 2982, <https://doi.org/10.5194/gmd-12-2961-2019>, 2019.

1059 R Core Team. (2013). R: A language and environment for statistical computing. [Available at  
1060 <http://www.r-project.org>.]

1061 Raymond, P. A., Hartmann, J., Lauerwald, R., Sobek, S., McDonald, C., Hoover, M., ...  
1062 Guth, P. (2013). Global carbon dioxide emissions from inland waters. *Nature*, 503(7476),  
1063 355–359. Retrieved from <https://doi.org/10.1038/nature12760>

1064 Regnier, P., Friedlingstein, P., Ciais, P., Mackenzie, F. T., Gruber, N., Janssens, I. A., ...  
1065 Thullner, M. (2013). Anthropogenic perturbation of the carbon fluxes from land to ocean.  
1066 *Nature Geosci*, 6(8), 597–607. Retrieved from <http://dx.doi.org/10.1038/ngeo1830>

1067 Ren, W., H. Tian, W.-J. Cai, S. E. Lohrenz, C. S. Hopkinson, W.-J. Huang, J. Yang, B. Tao,  
1068 S. Pan, and R. He (2016), Century long increasing trend and variability of dissolved organic  
1069 carbon export from the Mississippi River basin driven by natural and anthropogenic forcing,  
1070 *Global Biogeochem. Cycles*, 30, 1288–1299, doi:10.1002/2016GB005395.

1071 Reynolds, C., Jackson, T. & Rawls, W. Estimating available water content by linking 424 the  
1072 FAO soil map of the world with global soil profile databases and pedo-transfer 425 functions.  
1073 Am. Geophys. Union Fall Meet. EOS Trans. Spring Meet. Suppl. 80, S132 426 (1999).

1074 Richey, J. E., Melack, J. M., Aufdenkampe, A. K., Ballester, V. M., & Hess, L. L. (2002).  
1075 Outgassing from Amazonian rivers and wetlands as a large tropical source of atmospheric  
1076 CO<sub>2</sub>. *Nature*, 416(6881), 617– 620. <https://doi.org/10.1038/416617a>

1077 Schimel D, Stephens BB, Fisher JB. 2015.Effect of increasing CO<sub>2</sub> on the terrestrial carbon  
1078 cycle. *Proceedings of the National Academy of Sciences, USA* 112: 436–441

1079 Sheffield, J., Goteti, G., & Wood, E. F. (2006). Development of a 50-Year High-Resolution  
1080 Global Dataset of Meteorological Forcings for Land Surface Modeling. *Journal of Climate*,  
1081 19(13), 3088–3111. <https://doi.org/10.1175/JCLI3790.1>

1082 Silva, T.S.F., Costa, M.P.F. & Melack, J.M. Annual net primary production of macrophytes  
1083 in the eastern Amazon floodplain. *Wetlands* (2009) 29: 747. <https://doi.org/10.1672/08-107.1>

1084 Smith, W.K., Fox, A.M., MacBean, N., Moore, D.J.P. and Parazoo, N.C. (2020),  
1085 Constraining estimates of terrestrial carbon uptake: new opportunities using long-term  
1086 satellite observations and data assimilation. *New Phytol*, 225: 105-112.  
1087 doi:[10.1111/nph.16055](https://doi.org/10.1111/nph.16055)

1088 Spencer, R. G. M., P. J. Hernes, B. Dinga, J. N. Wabakanghanzi, T. W. Drake, and J. Six  
1089 (2016), Origins, seasonality, and fluxes of organic matter in the Congo River, *Global*  
1090 *Biogeochem. Cycles*, 30, 1105–1121, doi: 10.1002/2016GB005427.

1091 Sullivan, M. J. P., Talbot, J., Lewis, S. L., Phillips, O. L., Qie, L., Begne, S. K., ... Zemagho,  
1092 L. (2017). Diversity and carbon storage across the tropical forest biome. *Scientific Reports*, 7,  
1093 39102. Retrieved from <https://doi.org/10.1038/srep39102>

1094 Tathy, J. P., B. Cros, R. A. Delmas, A. Marengo, J. Servant, and M. Labat (1992), Methane  
1095 emission from flooded forest in central Africa, *J. Geophys. Res.*, 97(D6), 6159–6168,  
1096 doi:[10.1029/90JD02555](https://doi.org/10.1029/90JD02555).

1097 Tian, H., Q. Yang, R. G. Najjar, W. Ren, M. A. M. Friedrichs, C. S. Hopkinson, and S. Pan  
1098 (2015), Anthropogenic and climatic influences on carbon fluxes from eastern North America  
1099 to the Atlantic Ocean: A process-based modeling study, *J. Geophys. Res. Biogeosci.*, 120,  
1100 752–772, doi:10.1002/2014JG002760.

1101 [Tranvik, Lars J., Downing, John A., Cotner, James B., Loiselle, Steven A., Striegl, Robert](#)  
1102 [G., Ballatore, Thomas J., Dillon, Peter, Finlay, Kerri, Fortino, Kenneth, Knoll, Lesley](#)  
1103 [B., Kortelainen, Pirkko L., Kutser, Tiit, Larsen, Soren., Laurion, Isabelle, Leech, Dina](#)  
1104 [M., McCallister, S. Leigh, McKnight, Diane M., Melack, John M., Overholt, Erin, Porter,](#)  
1105 [Jason A., Prairie, Yves, Renwick, William H., Roland, Fabio, Sherman, Bradford](#)  
1106 [S., Schindler, David W., Sobek, Sebastian, Tremblay, Alain, Vanni, Michael J., Verschoor,](#)  
1107 [Antonie M., von Wachenfeldt, Eddie, Weyhenmeyer, Gesa A., \(2009\), Lakes and reservoirs](#)  
1108 [as regulators of carbon cycling and climate, \*Limnology and Oceanography\*, 54, doi:](#)  
1109 [10.4319/lo.2009.54.6 part 2.2298.](#)

1110 Tyukavina, A., Hansen, M. C., Potapov, P., Parker, D., Okpa, C., Stehman, S. V, ...  
1111 Turubanova, S. (2018). Congo Basin forest loss dominated by increasing smallholder  
1112 clearing. *Science Advances*, 4(11). <https://doi.org/10.1126/sciadv.aat2993>

1113 Valentini, R., Arneeth, A., Bombelli, A., Castaldi, S., Cazzolla Gatti, R., Chevallier, F., Ciais,  
1114 P., Grieco, E., Hartmann, J., Henry, M., Houghton, R. A., Jung, M., Kutsch, W. L., Malhi, Y.,  
1115 Mayorga, E., Merbold, L., Murray-Tortarolo, G., Papale, D., Peylin, P., Poulter, B.,  
1116 Raymond, P. A., Santini, M., Sitch, S., Vaglio Laurin, G., van der Werf, G. R., Williams, C.  
1117 A., and Scholes, R. J.: A full greenhouse gases budget of Africa: synthesis, uncertainties, and  
1118 vulnerabilities, *Biogeosciences*, 11, 381–407, doi:10.5194/bg11-381-2014, 2014

1119 Verhegghen, A., Mayaux, P., de Wasseige, C., & Defourny, P. (2012). Mapping Congo Basin  
1120 vegetation types from 300 m and 1 km multi-sensor time series for carbon stocks and forest  
1121 areas estimation. *Biogeosciences*, 9(12), 5061–5079. <https://doi.org/10.5194/bg-9-5061-2012>

1122 Viovy, N.. (2018). *CRUNCEP Version 7 - Atmospheric Forcing Data for the Community*  
1123 *Land Model*. Research Data Archive at the National Center for Atmospheric Research,  
1124 Computational and Information Systems Laboratory. <http://rda.ucar.edu/datasets/ds314.3/>

1125 Walker AP, De Kauwe MG, Medlyn BE, Zaehle S, Iversen CM, Asao S, Guenet B, Harper  
1126 A, Hickler T, Hungate BA et al. 2019. Decadal biomass increment in early secondary  
1127 succession woody ecosystems is increased by CO2 enrichment. *Nature Communications* 10:  
1128 454

1129 [Wang, Z. A., D. J. Bienvenu, P. J. Mann, K. A. Hoering, J. R. Poulsen, R. G. M. Spencer, and](#)  
1130 [R. M. Holmes \(2013\), Inorganic carbon speciation and fluxes in the Congo River, \*Geophys.\*](#)  
1131 [Res. Lett., 40, doi:10.1002/grl.50160](#)

1132 Weiss, L. C., Pötter, L., Steiger, A., Kruppert, S., Frost, U., & Tollrian, R. (2018). Rising  
1133 pCO<sub>2</sub> in Freshwater Ecosystems Has the Potential to Negatively Affect Predator-Induced  
1134 Defenses in *Daphnia*. *Current Biology*, 28(2), 327–332.e3.  
1135 <https://doi.org/https://doi.org/10.1016/j.cub.2017.12.022>

1136 Williams, C. A., Hanan, N. P., Neff, J. C., Scholes, R. J., Berry, J. A., Denning, A. S., and  
1137 Baker, D. A.: Africa and the global carbon cycle, *Carbon Balance and Management*, 2(3),  
1138 doi:10.1186/1750-0680-2-3, 2007.

1139 Yin, S., Li, X., & Wu, W. (2017). Comparative analysis of NPP changes in global tropical  
1140 forests from 2001 to 2013. *IOP Conference Series: Earth and Environmental Science*, 57(1),  
1141 12009. Retrieved from <http://stacks.iop.org/1755-1315/57/i=1/a=012009>

1142 Zhou, L., Tian, Y., Myneni, R. B., Ciais, P., Saatchi, S., Liu, Y. Y., ... Hwang, T. (2014).  
1143 Widespread decline of Congo rainforest greenness in the past decade. *Nature*, 509(7498), 86–  
1144 90. <https://doi.org/10.1038/nature13265>

1145 Zhuravleva, I., Turubanova, S., Potapov, P., Hansen, M., Tyukavina, A., Minnemeyer, S., ...  
1146 Thies, C. (2013). Satellite-based primary forest degradation assessment in the Democratic  
1147 Republic of the Congo, 2000-2010. *Environmental Research Letters*, 8(2), 24034.  
1148 <https://doi.org/10.1088/1748-9326/8/2/024034>

1149



1150

1151

1152

1153 *Appendix A*

1154

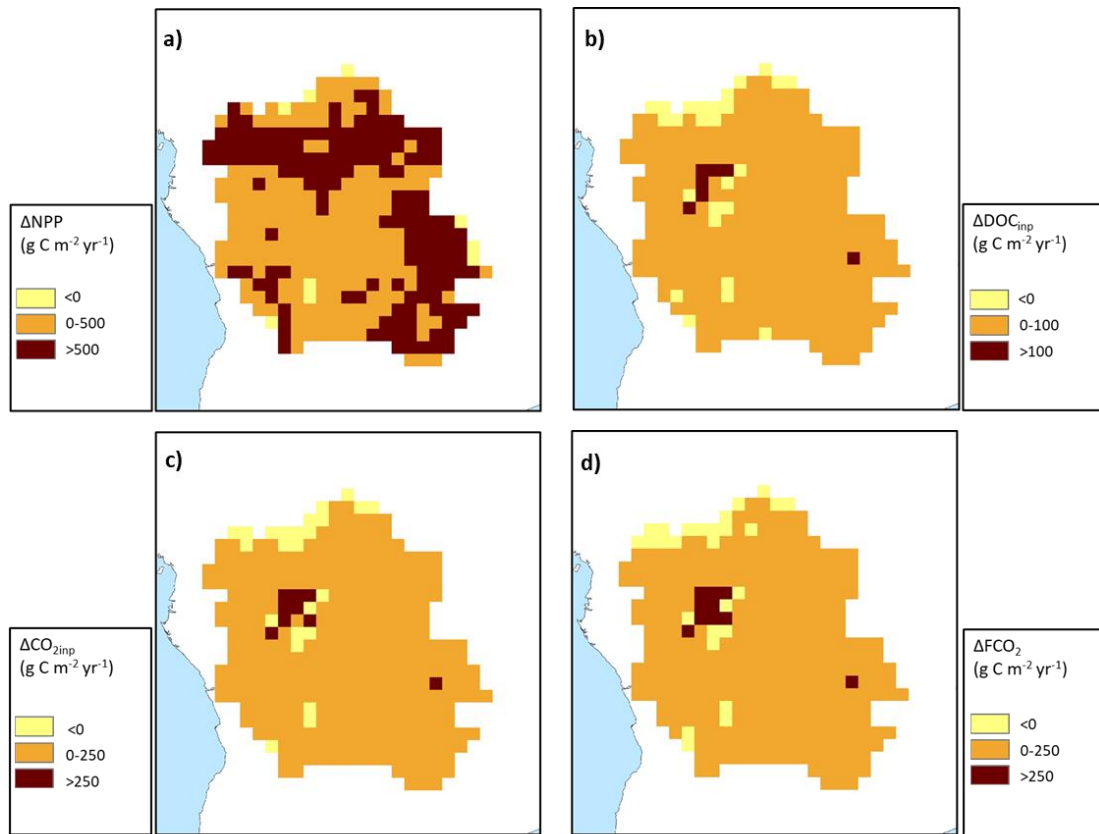
**Table A 1: Performance statistics for modelled versus observed seasonality of discharge on the Congo at Brazzaville**

Climate forcing	RSME	NSE	R <sup>2</sup>	Mean monthly discharge (m <sup>3</sup> s <sup>-1</sup> )
ISIMIP	29%	0.20	0.23	38,944
Princeton GPCC	40%	-0.25	0.20	49,784
GSWP3	46%	-4.13	0.04	24,880
CRUNCEP	65%	-15.94	0.01	16,394
Observed (HYBAM)				40,080

1155

**Table A 2: Pearson correlation coefficient (r) between detrended carbon fluxes and detrended climate variables**

	SHR	Aquatic CO <sub>2</sub> evasion	Lateral C	NEP	Rain	Temp.	MEI
NPP	-0.48	0.68	0.72	0.90	0.64	-0.57	-0.09
SHR		-0.41	-0.48	-0.71	-0.32	0.76	0.04
Aquatic CO <sub>2</sub> evasion			0.92	0.41	0.87	-0.30	-0.21
Lateral C				0.52	0.81	-0.38	-0.15
NEP					0.40	-0.74	-0.01
Rain						-0.31	-0.26
Temp.							0.03



1156

**Figure A 1:** Change ( $\Delta$ , 2099 minus 1861) in the spatial distribution of a) terrestrial NPP, b) DOC leaching into the aquatic system, c)  $\text{CO}_2$  leaching into the aquatic system and d) aquatic  $\text{CO}_2$  evasion. All at a resolution of  $1^\circ$

1157

1158

1159

1160

1161

1162

1163

1164

1165

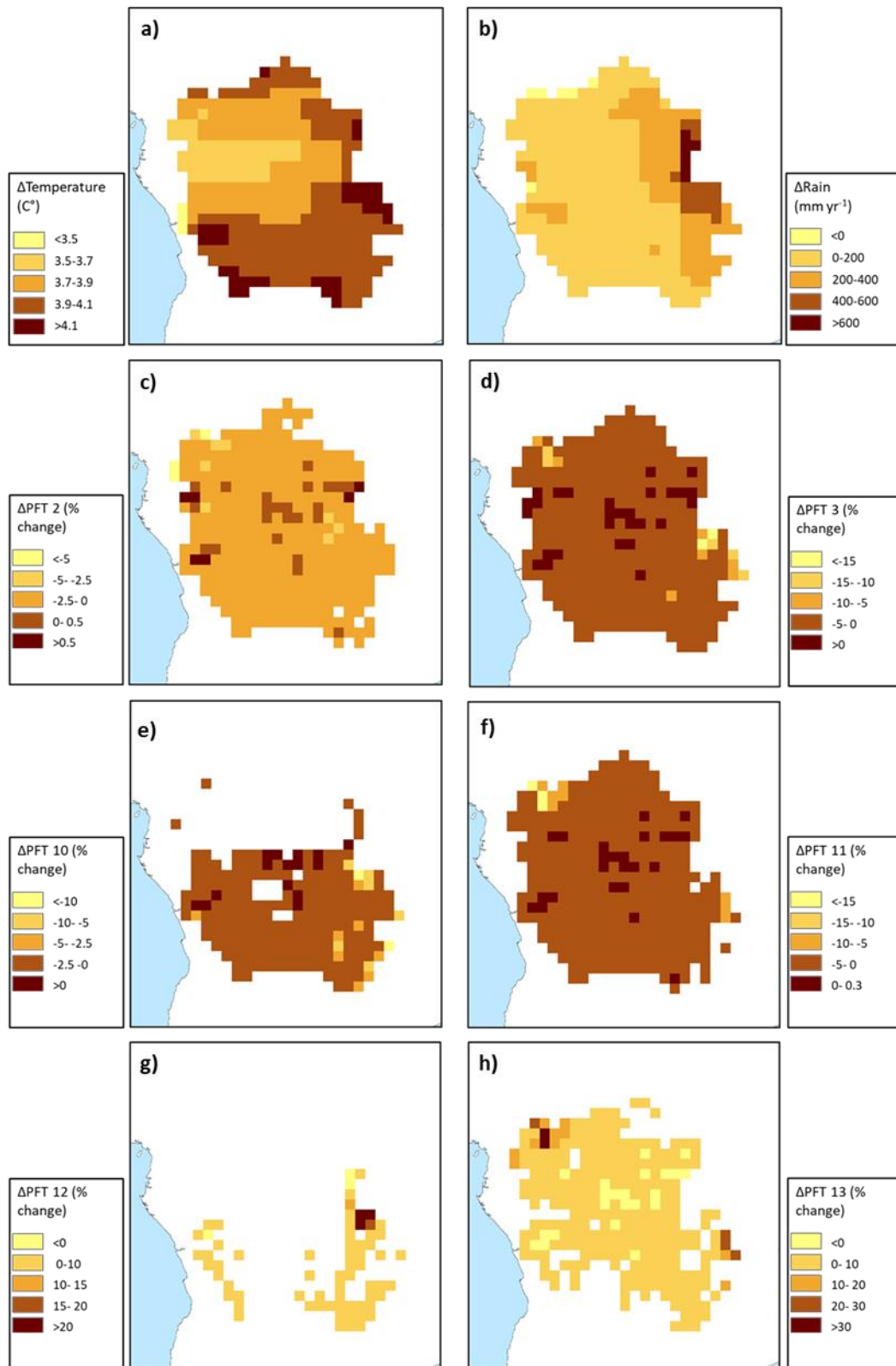


**Figure A 2:** Change ( $\Delta$ , 2099 minus 1861) in the spatial distribution of the principal climate and land-use drivers across the Congo Basin; a) mean annual temperature in  $^{\circ}\text{C}$ , b) mean annual rainfall in  $\text{mm yr}^{-1}$ , c)-h) mean annual maximum vegetated fraction for PFTs 2,3, 10,11,12 and 13. All at a resolution of  $1^{\circ}$ .

1167

1168

<b>Table A 3: Past (1861-1890), present-day (1981-2010) and future (2070-2099) mean values for important climate and land-use drivers across the Congo basin</b>								
Period	Temp.	Rain.	PFT2	PFT3	PFT10	PFT11	PFT12	PFT13
1861-1890	24.0	1451	0.263	0.375	0.154	0.254	0.015	0.014
1981-2010	25.2	1526	0.255	0.359	0.154	0.255	0.038	0.030
2070-2099	28.2	1654	0.258	0.362	0.147	0.245	0.039	0.037

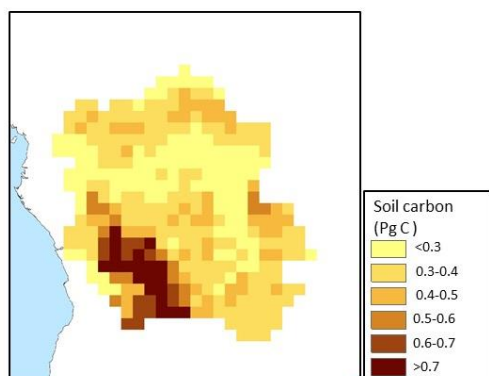


**Figure A 3: Spatial distribution of simulated total carbon stored in soils for the present day (1981-2020).**

1169

1170

1171